Evidence for an upper mantle plume beneath the Tanzanian craton from Rayleigh wave tomography

Dayanthie S. Weeraratne, Donald W. Forsyth, and Karen M. Fischer
Department of Geological Sciences, Brown University, Providence, Rhode Island, USA

Andrew A. Nyblade
Department of Geosciences, Pennsylvania State University, University Park, Pennsylvania, USA

Received 28 October 2002; revised 22 March 2003; accepted 12 May 2003; published 16 September 2003.

[1] The Archean Tanzanian craton, nestled between the eastern and western branches of the East African Rift, presents a unique opportunity to study the interaction of active rifting with stable cratonic lithosphere. The high density of Rayleigh wave paths recorded in a regional seismic array yields unusually precise determinations of phase velocity within the Tanzanian craton. Shear velocities in the cratonic lithosphere are higher than a global average to a depth of 150 ± 20 km. Beginning at 140 km, shear velocity decreases sharply, reaching a minimum of 4.20 ± 0.05 km/s at depths of 200–250 km. The base of the lithosphere, identified by the depth to the center of the maximum negative velocity gradient, is similar to that found beneath other Archean lithospheres. Where Cenozoic rifting crosscuts the southern corner of the craton, velocities up to 130 km depth are reduced, indicating recent disruption of the lithosphere. The anomalously low velocities beneath the Tanzanian craton indicate high temperatures and the presence of melt, consistent with the spreading of a mantle plume head beneath the craton. Tests for the possibility of a radial pattern of azimuthal anisotropy that may indicate outward flow from a plume show that a model with average anisotropy of 0.71 ± 0.17% centered SE of Lake Victoria fits the data significantly better than a uniform, single direction of anisotropy. Thus our results agree with the suggestion that an upper mantle plume, centered beneath the Tanzanian cratonic lithosphere, provides the buoyancy required for uplift of the East African Plateau. *INDEX TERMS:* 7218 Seismology: Lithosphere and upper mantle; 7255 Seismology: Surface waves and free oscillations; 8120 Tectonophysics: Dynamics of lithosphere and mantle—general; 8180 Tectonophysics: Tomography; 8109 Tectonophysics: Continental tectonics—extensional (0905); *KEYWORDS:* Archean craton, Tanzania, surface waves, low-velocity zone

Citation: Weeraratne, D. S., D. W. Forsyth, K. M. Fischer, and A. A. Nyblade, Evidence for an upper mantle plume beneath the Tanzanian craton from Rayleigh wave tomography, *J. Geophys. Res.*, *108*(B9), 2427, doi:10.1029/2002JB002273, 2003.

1. Introduction

[2] The stable interiors of continental plates are estimated to have survived tectonic activity spanning nearly half of Earth's history, demonstrating resistance to collisional events, adjacent plate subduction, suturing, dissection, amalgamation, and intraplate volcanism. The crustal rocks at the surface of many of these continental cratons are Archean in age [e.g., *Cahen et al.*, 1984; *Condie*, 1994], as are samples from the underlying lithospheric mantle [e.g., *Lee and Rudnick*, 1999; *Chesley et al.*, 1999; *Irvine and Pearson*, 2001]. Periodic disbanding and reconvening of large landmasses since the Archean, however, suggest the importance of continental rifting in lithosphere evolution. The Tanzanian craton, set between active branches of the East African Rift system, is at present influenced by continental rifting and possibly a mantle plume [*Nyblade and Robinson*, 1994; *Simiyu and Keller*, 1997; *Prodehl et al.*, 1997; *McNutt*, 1998; *Ritsema et al.*, 1999]. Much debate and contradictory evidence exists regarding the thickness of the lithosphere and whether it has been eroded. Seismic tomography studies thus far have been unable to resolve anomalous buoyant velocity structure in the upper mantle that could provide an explanation for the uplift of the broad, East African Plateau. We will present surface wave data with better vertical resolution of local velocity structure than previous seismological studies in an attempt to resolve controversies about lithospheric thickness, compare the structure of the Tanzanian craton to a global sampling of Archean lithospheres, and provide evidence for the presence of an upper mantle plume beneath the Tanzanian craton that may be the source of uplift for the East African Plateau.

[3] The Tanzanian craton, centrally located within the East African Plateau, spans an area of over 350,000 km^2 and has an average elevation of 1260 m. The Archean age craton (Figure 1) is composed of greenstone belts and granitoids more than 2500 Myr old [*Cahen et al.*, 1984].

0148-0227/03/2002JB002273$09.00

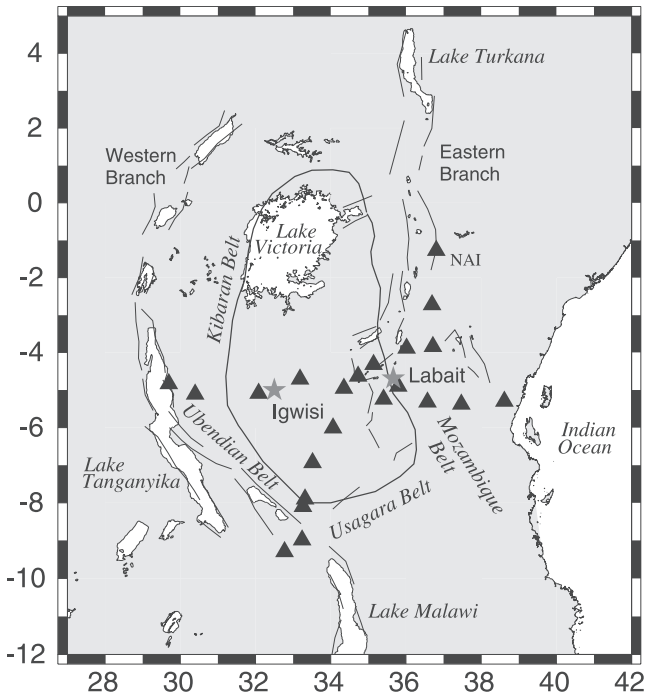

Figure 1. Tectonic map of East Africa. Tanzanian craton boundary (solid black outline) is centered between the western branch and the eastern branch of the East African Rift system (line segments). Solid triangles indicate station locations for the Tanzanian Broadband Seismic Network. Stars show locations of the Labait and Igwisi volcanoes discussed in the text.

The stable craton has endured numerous collisional events resulting in a complex pattern of mobile belts surrounding its perimeter. The Usagara and Ubendian belts, formed in the early Proterozoic, lie southeast and southwest of the craton, respectively; the Mozambique and Kibaran belts, formed by younger, late Proterozoic collisional events, oppose each other to the east and west. Cenozoic extensional rifts (solid line segments in Figure 1) skirt the eastern and western sides of the elongated craton boundary. NE-SW trending normal faults are also observed at the southern edge within the craton, adjacent to the Usagara belt with initial rupture ages estimated as recent as mid-Pliocene [*Ebinger et al.*, 1989b]. The volume of igneous basalt in the eastern branch of the East African Rift system, estimated at greater than 900,000 km^3 [*Morley*, 1999], far exceeds that of the western branch. Seismicity is less frequent in the eastern branch and tends to originate at shallower depths [*Fairhead and Girdler*, 1971; *Camelbeeck and Iranga*, 1996; *Nusbaum et al.*, 1993; *Foster and Jackson*, 1998]. Volcanic activity initiated about 36 Ma in the eastern branch near Lake Turkana and is dated progressively younger toward the south. Volcanism in the western branch initiated later, ~13 Ma [*Ebinger et al.*, 1989b; *Foster and Jackson*, 1998; *Kampunzu et al.*, 1998]. *Nyblade and Brazier* [2002] suggest that the formation of the two rift branches is tectonically linked, that the southward propagation of the eastern branch stopped when it encountered the Tanzanian craton, and that it jumped to the west side of the craton creating the western branch in order to accommodate extensional stresses.

[4] Geophysical and geological studies of the East African Plateau have focused on lithospheric thickness, the impact of rifting on cratonic lithosphere and the source of anomalous uplift. Using the global tomography models of *Zhang and Tanimoto* [1993] and *Grand* [1994], *Polet and Anderson* [1995] found that the Archean shields of North America, western Europe, and west Africa have deep continental roots extending to depths of 300–450 km but that the central African lithosphere, consisting of the Congo and Tanzanian cratons, is only 100–200 km thick. By comparison, a study of compressional (*P*) and shear (*S*) wave travel time data [*Ritsema et al.*, 1998] from the Tanzanian Broadband Experiment [*Owens et al.*, 1995; *Nyblade et al.*, 1996] identified positive velocity anomalies within the mantle lithosphere extending to depths of 200–350 km. In sharp contrast to the high-velocity craton, low-velocity anomalies were reported beneath the eastern and western branches extending to depths of at least 400 km. *Ritsema et al.* [1998] found no evidence for low velocities shallower than 400 km beneath the craton and attributed the buoyancy source for the elevated plateau to structure at depths beyond their resolution.

[5] A recent surface wave tomography study of fundamental mode Rayleigh waves was compiled from several data sets, including the Tanzanian Broadband Experiment, throughout the African continent, and these data were inverted for shear wave velocities yielding a lateral resolution of about 500 km [*Ritsema and van Heijst*, 2000]. *Ritsema and van Heijst* [2000] identified high-velocity structures of three major cratonic bodies beneath western, central, and southern Africa extending to a common depth of approximately 250 km, but thinning by 50–80 km beneath the Tanzanian craton. Another surface wave study included higher-mode Rayleigh waves, providing improved depth resolution of upper mantle structure, particularly within the transition zone [*Debayle et al.*, 2001], but with fewer paths and poorer lateral resolution in the vicinity of Tanzania than *Ritsema and van Heijst* [2000]. A lithospheric thickness of approximately 200 km was reported with high shear wave velocities in the 250–450 km depth range beneath the Tanzanian craton. High velocities at depths greater than 400 km are not in agreement, however, with receiver function studies [*Owens et al.*, 2000], which suggest that a thin upper mantle transition zone is caused by downward deflection of the 410-km discontinuity. *Nyblade et al.* [2000] proposed a 200–400 km wide thermal mantle anomaly beneath the East African Rift and part of the Tanzanian craton extending from the base of the lithosphere well into the transition zone.

[6] In a model that assumes isostatic equilibrium and integrates results from gravity and topography studies, active-source seismic studies, passive teleseismic body wave tomography, and geothermometry and geobarometry from mantle xenoliths, *Simiyu and Keller* [1997] estimated a lithospheric thickness of about 130 km beneath the Tanzanian craton. Their model predicted low-density anomalies of ~1% in the asthenosphere immediately beneath the lithosphere. Coherence and admittance analysis of gravity and topographic anomalies for lithospheric plate flexure showed that an isostatically compensated plateau does not fully

account for the magnitude of the long-wavelength negative Bouguer gravity anomaly in the region and additional buoyancy forces from the deeper mantle may be required [*Ebinger et al.*, 1989a]. The effective elastic thickness of the cratonic lithosphere is significantly greater than in the Proterozoic orogenic belts or rifts [*Ebinger et al.*, 1997].

[7] Petrological and geochemical studies also provide estimates of lithospheric thickness beneath the Tanzanian craton. Peridotite xenoliths from the Quaternary Labait volcano located on the eastern margin of the craton at its intersection with the eastern branch of the rift indicate that refractory mantle with Re depletion ages of ~2.8 Ga persists to at least 150 km depth [*Chesley et al.*, 1999; *Lee and Rudnick*, 1999]. However, beginning at depths of 120–140 km, more fertile xenoliths are evident with deformed textures and much younger Re depletion ages. These garnet-bearing xenoliths define a steeper geothermal gradient than the refractory samples and the high proportion of dense, Fe-rich dunites in the xenolith population indicate that the lower cratonic lithosphere is interacting chemically and thermally with asthenospheric magmas [*Lee and Rudnick*, 1999]. Interaction with magma and thermal reequilibration at depths of about 140 km suggests that we might expect a corresponding decrease in shear velocity, although there is a question of whether this thickness applies to the craton as a whole or just the portion of the lithosphere beneath Labait volcano that is currently interacting with the eastern rift branch. *Ebinger et al.* [1997] suggested that a mantle plume has thermally eroded the eastern margin of the Tanzanian cratonic lithosphere over the last 40–50 Myr. In the interior of the craton, study of diamondiferous, Palaeogene kimberlites suggest a lithospheric thickness of 170–200 km [*Griffin et al.*, 1993], while analysis of the youngest magmatic rocks on the craton from the Quaternary Igwisi hills indicates only that the magma formed at depths of at least 110 km [*Dawson*, 1994].

[8] As described above, there are inconsistent estimates of lithospheric thickness beneath Tanzania and of the existence and depth extent of low asthenospheric seismic velocities. One problem is that while body wave tomography studies obtain good lateral resolution of mantle structure, vertical resolution is often compromised due to steeply incident ray paths. Surface wave studies may provide better vertical resolution in the upper 200 km, but large-scale or global tomographic studies may have limited horizontal resolution due to low density of crossing ray paths or smoothing of short-wavelength heterogeneity. Another problem is inconsistencies in the definition of lithospheric thickness. Many studies have identified the base of the lithosphere as the maximum depth of a high-velocity anomaly and may overestimate lithospheric thickness if vertical smearing is present. We adopt the definition of the lithospheric base as the depth to the center of the maximum negative velocity gradient, which provides a better measure if a sharp transition or steep gradient is vertically smeared. We seek to improve the resolution of the lithosphere beneath the Tanzanian craton using Rayleigh wave data recorded by the Tanzanian Broadband Experiment. Vertical resolution is improved by obtaining more precise phase velocities using a method that accounts for the distortion of the incoming wave field by heterogeneities outside the array [*Forsyth et al.*, 1998; D. W. Forsyth and A. Li, Array analysis of two-dimensional variations in surface wave phase velocity and azimuthal anisotropy in the presence of multipathing interference, submitted to AGU Geophysical Monograph, 2003 (hereinafter referred to as FL)]. Horizontal resolution is improved by employing a local seismic array that focuses on the primary target area with a high density of crossing ray paths. We find that the lithosphere of the Tanzanian craton is similar in thickness to other Archean lithospheres but is underlain by a low-velocity zone (LVZ) that indicates high temperatures and the presence of partial melt, perhaps associated with an upper mantle plume.

2. Surface Wave Observations and Model Parameterization

[9] Rayleigh wave seismic data were obtained from the Tanzania Broadband Seismic Network deployed from June 1994 to May 1995. The array consisted of two lines of stations extending E-W and approximately NNE-SSW intersecting at the interior of the craton southeast of Lake Victoria (Figure 1). The total array spanned approximately 900 km with station spacing between 50 and 200 km. Although two-dimensional surface wave tomography would benefit from a more grid-like array distribution, intersecting ray path coverage in this experiment does allow for some resolution of lateral heterogeneity. The temporary deployment consisted of 21 broadband stations with up to 20 operational at any one time. To improve ray path coverage to the north, we add records from GSN station, NAI, located in Nairobi, Kenya. We make timing corrections to various stations consistent with the experiment data report. In addition, a frequency-dependent amplitude and phase correction is applied to GOMA, the westernmost station, during the months in 1995 when station response differed from the standard.

[10] We use a total of 93 events at distances ranging from 30° to 120° with magnitude $M_s \geq 5.9$. Earthquake depths range from 8 to 239 km with only a few events deeper than 100 km. Complete azimuthal distribution is ideal for maximizing the density of crossing ray paths and resolving azimuthal anisotropy. The azimuthal distribution of events (Figure 2a) is good, although few events occur at NW and SE azimuths. Path coverage varies somewhat with frequency (see Table 1) due to decreasing signal-to-noise ratio at long periods and multipath interference at short periods (Figures 2b and 2c). Ray path density at long periods is similar to that at 50 s. Although there are fewer paths at short periods, the pattern of coverage is almost the same, so there should be little or no bias introduced by changing geographic coverage, just larger uncertainties due to less redundancy.

[11] Rayleigh waves have high signal-to-noise ratios and their dispersion (Figure 3a) constrain vertical variations in shear velocity. Sensitivity kernels presented in the inset of Figure 3a show that total sensitivity to changes in shear velocity is distributed over a broad depth range but peak sensitivity occurs at a depth of approximately one third of the wavelength. We measure Rayleigh wave phase velocities at 12 frequencies, ranging from 7 to 50 mHz. Each frequency is analyzed separately. We first filter the Rayleigh wave with a 10-mHz-wide, zero-phase-shift, band-pass

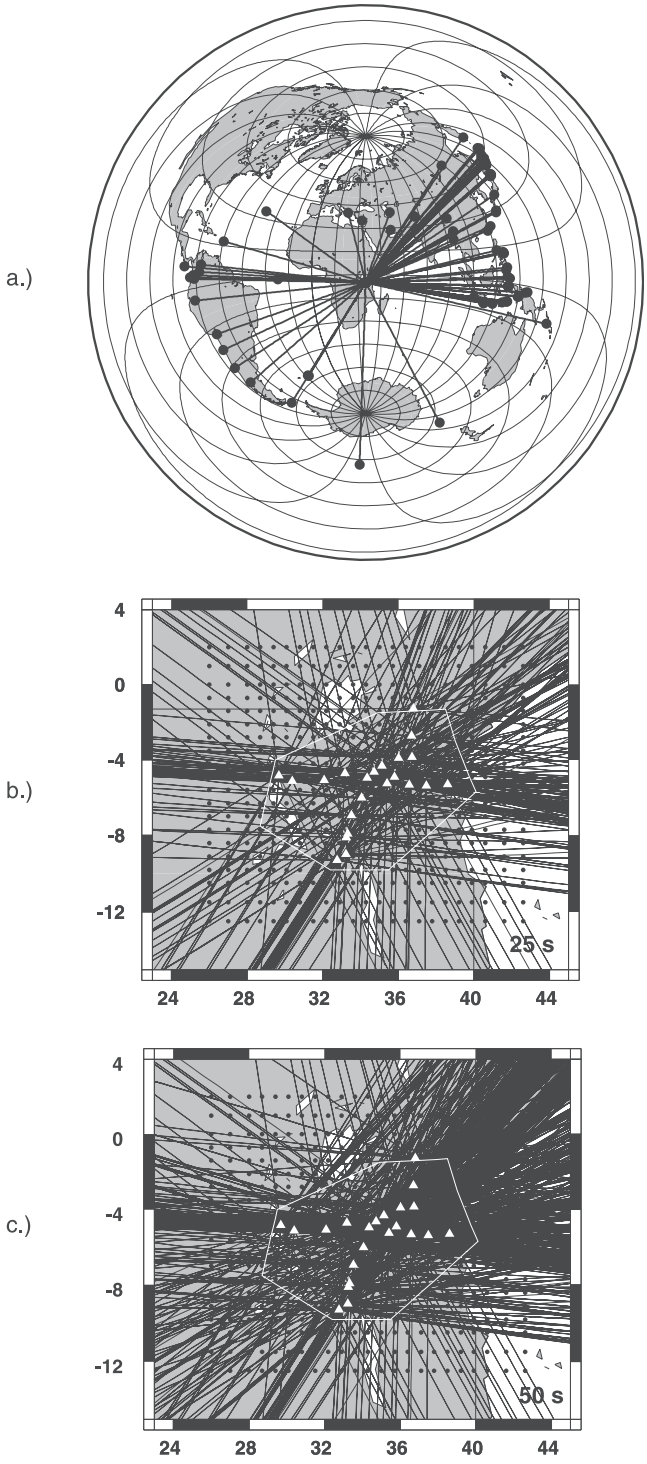

Figure 2. (a) Azimuthal distribution of seismic events used in this study. (b) Ray path coverage at 25 s. White outline denotes the region with best crossing path density. Stations are shown by open triangles. (c) Ray path coverage at 50 s.

filter centered at the frequency of interest (Figure 3a) in order to evaluate the signal-to-noise ratio in that band. A time window is then selected to isolate the desired signal and to eliminate noise and body wave signals outside the window. The same window length is employed for every station of each event-frequency pair, centered on the expected group arrival time.

[12] Most events have variations in amplitude or waveform across the array (Figure 3b) that are indicative of focusing or multipath propagation between the source and the array caused by lateral heterogeneities [*Friedrich et al.*, 1994]. In our tomographic inversion for phase velocity, we account for these perturbations in the wave field due to non-great circle path propagation with a two-plane wave approximation [*Forsyth et al.*, 1998; FL]. This approximation allows for complexity in the incoming wave field not considered in standard tomographic techniques but does not have the burden of inverting for a large number of parameters by requiring that the wave field be represented by a series of basis functions [*Friedrich et al.*, 1994]. Perturbations in the wave field are represented by the interference of two plane waves of the form

$$U_z(\omega) = A_1(\omega)\exp[-i(\mathbf{k}_1 \cdot \mathbf{x} - \omega t)] + A_2(\omega)\exp[-i(\mathbf{k}_2 \cdot \mathbf{x} - \omega t)], \quad (1)$$

where $U_z(\omega)$ is vertical displacement, $\mathbf{k}_i$ is the horizontal wave number for each wave, $\mathbf{x}$ is the position vector, and t is time. The initial phase at a reference station, amplitude (A_i) and direction for each of the two plane waves are the model parameters in addition to the anisotropic phase velocity coefficients (B_i) at each nodal point. The advantage of this method over the usual approach of ignoring interference effects, i.e., the one-plane wave method for local array analysis, is that it provides a 30–40% reduction in variance of phase or travel time compared to tomography with the one-plane wave method [*Li et al.*, 2003].

[13] We assume the azimuthally anisotropic phase velocity, C, depends on frequency, ω, and azimuth, θ,

$$C(\omega, \theta) = B_o(\omega) + B_1(\omega)\cos 2\theta + B_2(\omega)\sin 2\theta, \quad (2)$$

where B_o is the azimuthally averaged phase velocity. We assume higher-order terms are small for Rayleigh wave propagation [*Smith and Dahlen*, 1973]. Phase velocities are described by Gaussian weighted averages of the characteristic velocity at grid nodes spaced 0.7° apart throughout the region shown in Figure 4. Two rows of nodes surrounding the primary region spaced 1° apart absorb travel time variations not accounted for by the two-plane wave approximation.

Table 1. Resolution for Phase and Shear Wave Velocity Inversions

Period, s	Number of Paths	RMS Phase Misfit, s
20	356	2.06
22	390	1.88
25	384	2.25
29	828	1.90
33	965	1.87
40	946	1.94
50	1051	2.23
67	1128	1.51
80	1025	1.74
100	866	2.04
125	806	2.10
143	800	2.80

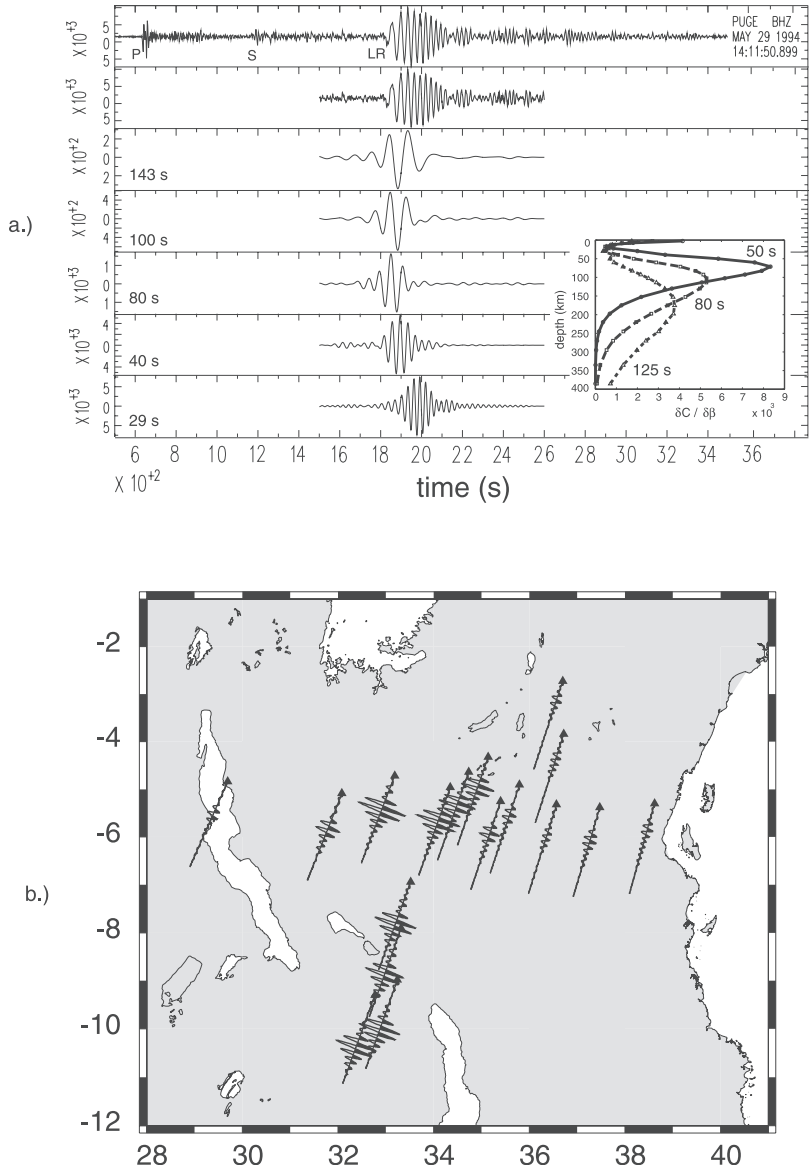

Figure 3. (a) Dispersion for an event recorded at station, PUGE. Filters have band width of 0.01 Hz and range from 7 to 50 mHz. The arrivals of the *P*, *S*, and Rayleigh waves (LR) are indicated. The inset shows sensitivity kernels for periods 50 s (solid line), 80 s (dashed line), and 125 s (short dashed line). Each period has peak sensitivity at depth approximately one third wavelength but is influenced by structure in a broad depth range. (b) Seismograms observed at the array of stations for a magnitude, M_s = 6.1, event originating from Turkmenistan NNE of the map location. The records are filtered at 50 s and a common window is cut around the Rayleigh wave phase. Record azimuth is oriented in the direction of the great circle path. Note that the Rayleigh wave arrives later at the stations farthest from the event and that there are strong amplitude variations, indicating focusing and defocusing or multipath interference.

[14] In the inverse problem, the phase and amplitude of each filtered and windowed seismogram are determined through Fourier analysis and provide two pieces of information for each record event at each station. It is necessary to have at least four station records for each event to solve for the six wave parameters and still provide any information about the velocity. Additional records provide better resolution of the wave field parameters and information about lateral or azimuthal variations in phase velocity. We use a minimum of 7 and maximum of 20 records per event depending on signal quality and station operations. As described by FL, we first solve the nonlinear problem of obtaining the best fitting wave parameters (equation (1)) using a simulated annealing method while holding velocity fixed. Then a linearized inversion [*Tarantola and Valette*, 1982] is used to solve for corrections to the velocity model and perturbation to the wave parameters simultaneously. Observed interference effects for the wave field are shown in Figure 3b for a magnitude, M_s = 6.9, event from Turkmenistan. We attribute amplitude variations to constructive and destructive interference.

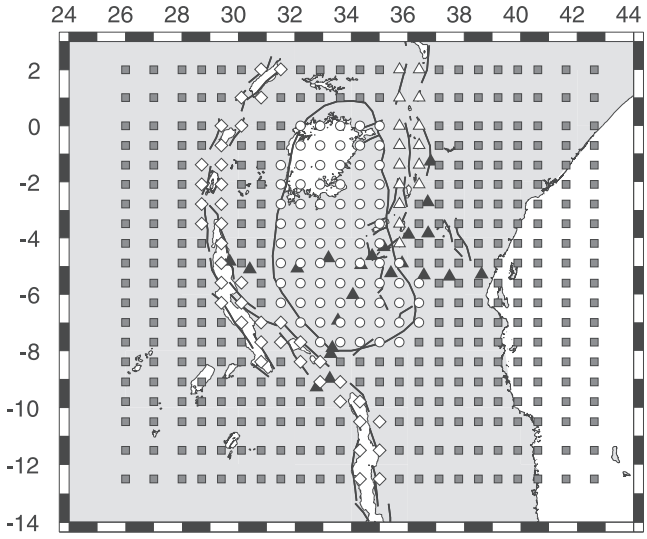

Figure 4. Grid node locations designated for phase velocity inversions. The craton is designated by circles, western branch is designated by diamonds, eastern branch is designated by triangles, and background is designated by shaded squares. Grid node spacing is described in the text.

[15] To account for frequency-dependent scattering in the wave field [e.g., *Gudmundsson*, 1996; *Marquering et al.*, 1998; *Spetzler and Snieder*, 2001], we apply a frequency-dependent smoothing length for the velocity field to widen the region of sensitivity about the great circle path as the wavelength, λ, increases. The width of the Fresnel zone, x_f, is described by a time delay of $\delta t < T/4$, where T is the period, for an incoming plane wave [*Gudmundsson*, 1996], giving

$$x_f = \sqrt{2L\lambda + \frac{\lambda^2}{4}}. \quad (3)$$

In our regional array, the typical propagation distance, $L \geq \lambda$, and the Fresnel zone width can be approximated by $x_f = \sqrt{2L\lambda}$. We thus apply a characteristic smoothing length, $L_w = x_f/2\sqrt{2}$ such that 95% of the cross sectional area under a Gaussian weighting or sensitivity function is within the first Fresnel zone. Further work is necessary, however, for a more formal treatment of scattering effects within the array in our method.

3. Phase Velocity Results

[16] We present our results first for Rayleigh wave phase velocity and then invert for shear wave velocity in a layered Earth model in section 4. In preliminary inversions, we solve for the best uniform phase velocity within the entire study area (described by all the grid nodes) at each period. The uniform velocity is then used as the starting model in subsequent inversions for geologically distinct regions such as the craton or rifts. Finally, we use these regional velocities as starting models for a full two-dimensional inversion to test for significant variations from the regional models. All initial inversions for this study assume isotropic phase velocities. A series of inversions that consider azimuthal anisotropy are also presented. Polarization anisotropy is not constrained as we do not yet incorporate Love wave phase velocities.

[17] In the regional pure path models, grid nodes are divided into four geologic regions, as designated in Figure 4, on the basis of the boundaries defined by greenstone belts and granitoids for the Tanzanian craton and normal faults in the eastern and western branches of the East African Rift. The remaining grid points are assigned to a background category which encompasses all other tectonic structures. Grid node velocities in each geologic region are required to vary as a group giving the phase velocity for that region which provides the best fit to the data in a least squares sense. Phase velocities as a function of period for each geologic area are plotted in Figure 5a. Velocities, in general, are highest in the craton, followed by the background group and the western branch. The lowest velocities are observed in the eastern branch at nearly all periods. The change in slope at ~33 s indicates a change from sensitivity to both crust and mantle structure at short periods to primarily mantle sensitivity at longer periods. Phase velocities in the craton are well constrained with typical standard deviations of 0.1% shown to be smaller than the symbol in Figure 5a. Phase velocity fluctuations with period in both rifts are fairly large due to larger standard deviations but may be smoothly varying within the confidence limits. The rifts are clearly lower in velocity than the craton, but how much lower depends somewhat on the assumed width or number of grid nodes assigned to these regions. Thus our primary emphasis is on cratonic structure rather than rift structure.

[18] A close look at the craton profile shows smoothly increasing velocities between 25 and 40 s and then a flattening of the dispersion curve (Figure 5b) as compared to the phase velocities for the Canadian shield [e.g., *Brune and Dorman*, 1963; *Ekstrom et al.*, 1997] over a period range between 50 and 100 s. We compiled phase velocity curves (Figure 5d) from a global surface wave model [*Ekstrom et al.*, 1997] for regions representing Archean cratons (Figure 5c). Our choice of Archean continental regions is based on resolution of the global model where structure up to degree 20 (~1000 km wavelength) is recoverable. Only the area for the Kaapvaal craton (~750 km × 950 km) is below this limit, as is the Tanzanian craton. Although there is variability in global surface wave coverage, dispersion curves averaged over these large regions should give reliable estimates of frequency-dependent phase velocity. The lithosphere of the Kaapvaal, Canadian, western Siberian (Anabar), and Yilgarn cratons are identified by phase velocities that are higher than the global average PREM model [*Dziewonski and Anderson*, 1981] at short periods and are consistently high for long periods up to 150 s. Rayleigh wave velocities in the Indian, east Siberian, and Sino-Korean cratons are lower than PREM at short periods and follow the global average at long periods. The dispersion curve for the Sino-Korean craton is either close to or lower than PREM at nearly all periods and suggests the absence of thick cratonic lithosphere. The phase velocity curve for the Indian shield is most similar to the Tanzanian craton displaying high velocities at periods less than 50 s, a reduced slope between 50 and 100 s and PREM-like velocities at the longest periods. The unique dispersion curve for the Tanzanian craton displays a nearly constant phase velocity in

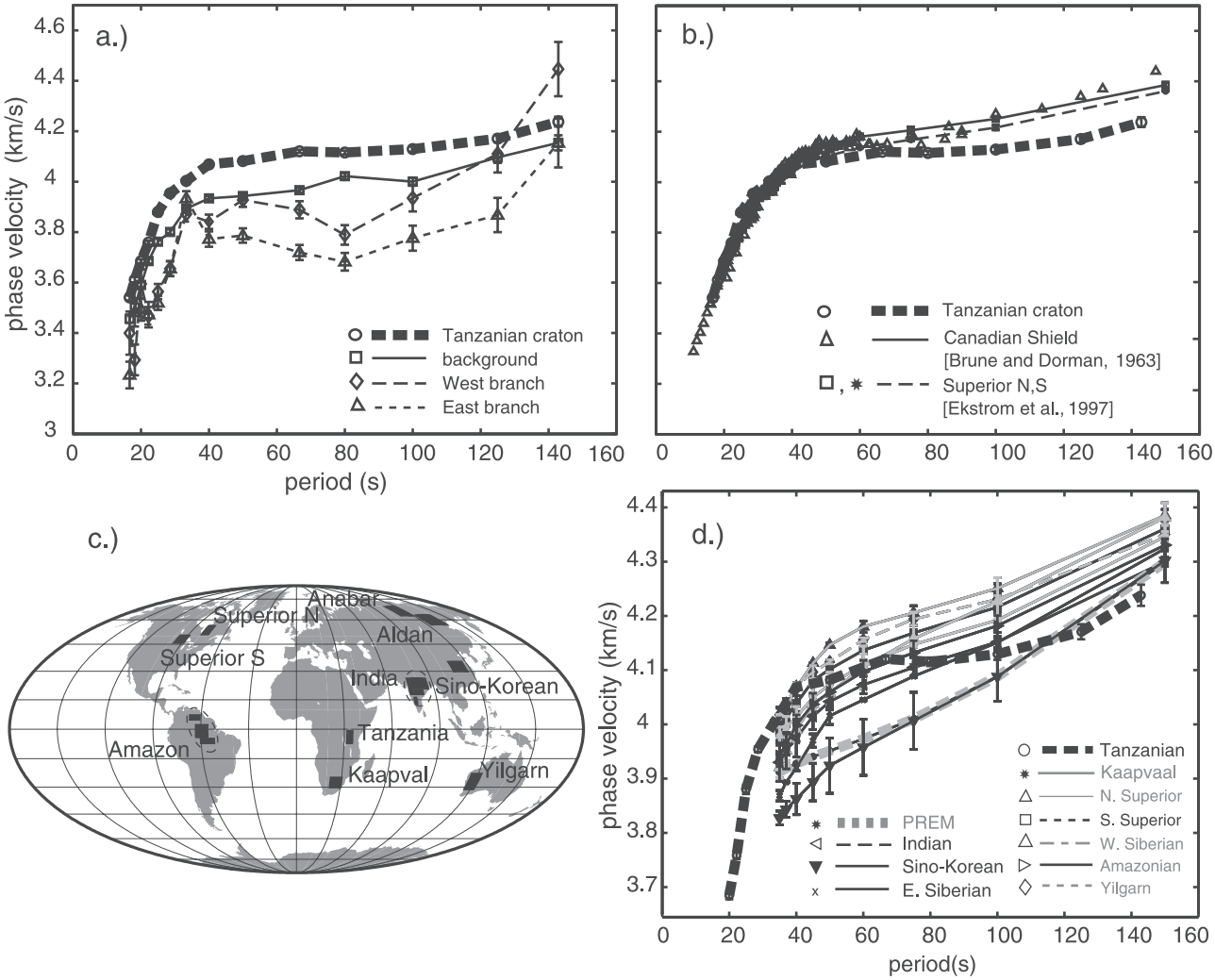

Figure 5. (a) Phase velocities for geologic areas designated as in Figure 4. Four geologic areas are identified: craton (circles), western branch (diamonds), eastern branch (triangles), and background (squares). Standard deviation of phase velocity within each region is shown. Phase velocities for the craton have standard deviations of only 0.1–0.2% and are smaller than the symbol at nearly all periods. (b) Tanzanian craton dispersion curve plotted with phase velocities from a local surface wave study within the Canadian shield (triangles) [*Brune and Dorman*, 1963], and velocities taken from a global phase velocity model (squares and asterisks) [*Ekstrom et al.*, 1997]. (c) Archean craton regions used in compiling phase velocities from the global phase velocity model. (d) Dispersion curves for Archean cratons obtained from the surface wave global model [*Ekstrom et al.*, 1997] plotted with phase velocities for the Tanzanian craton from this study. Error bars for global velocities indicate variations or gradients in the global model across the indicated region.

the midperiod range and has lower phase velocities than PREM above 100 s. Inversions for shear wave velocity described in section 4 will demonstrate that the low phase velocities in the Tanzanian craton observed for the periods between 50 and 100 s are due to a low-velocity zone in the upper mantle.

[19] Lateral variations in phase velocity are obtained by using phase velocity results from the four geologic areas as a starting model and allowing the velocity at each grid node in the inversion to vary. Although the configuration of the array is not ideal for conventional, two-dimensional tomography, there is some resolvable information about velocity variations in addition to those between the four geologic areas. The starting model is shown in Figure 6a with highest phase velocities assigned to the craton region, lower velocities in the western and eastern branches, and intermediate velocities for the background. The starting model has smooth transitions between regions because the velocity at each point in the map represents a weighted average of neighboring grid nodes using a 2-D Gaussian weighting function with characteristic length, L_w, as described in section 2. The velocities are masked where confidence limits dictated by standard error contours in Figure 6c show that resolution is limited.

[20] Two-dimensional phase velocity variations are shown in Figure 6b for a 50 s period inversion. As expected,

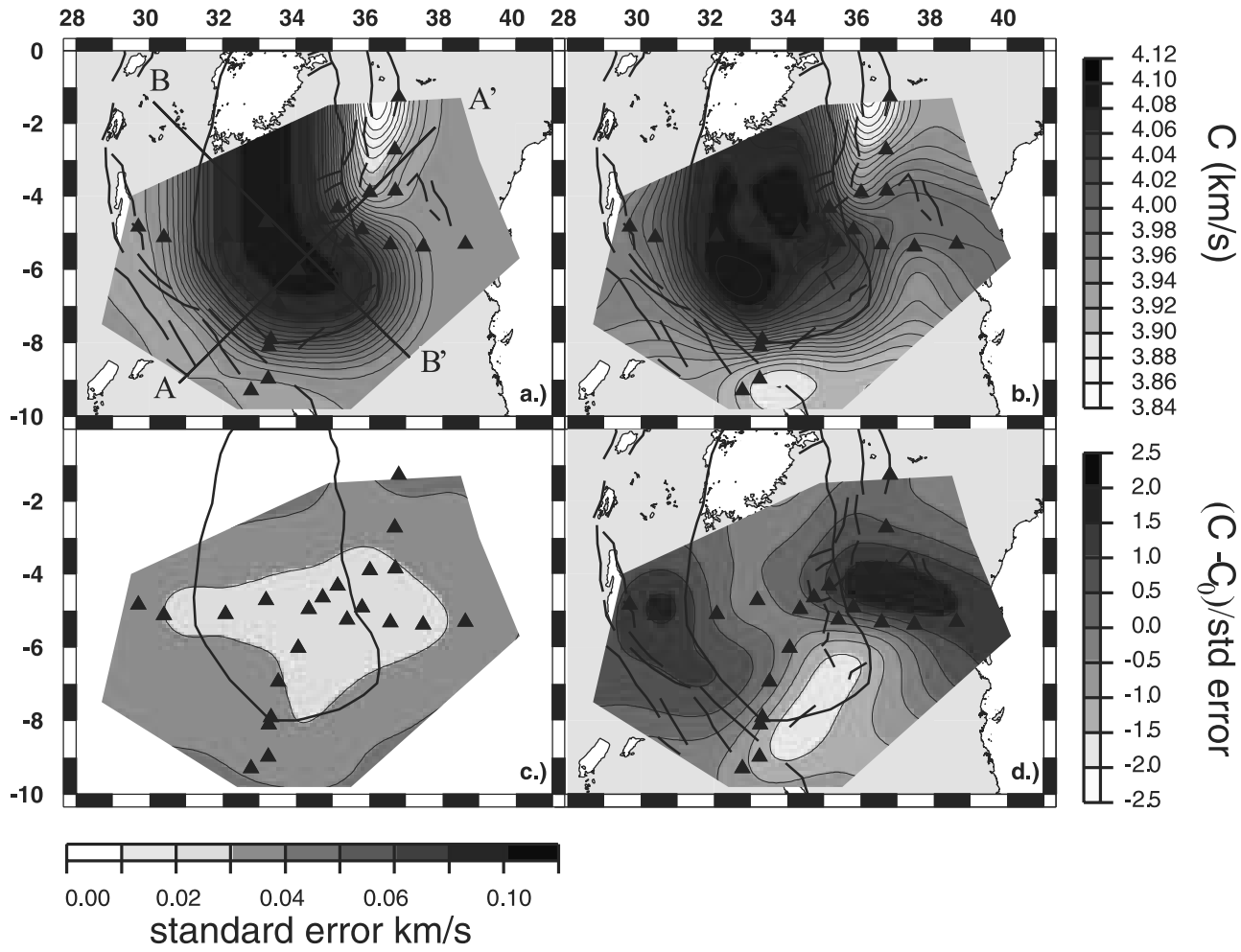

Figure 6. Phase velocity map for 2-D inversion at 50 s. Tanzanian craton outline and rift segments are shown as in Figure 1. Masked region represents area of best ray path coverage. (a) Starting model for 2-D inversions. Starting velocities are uniform for each region: craton, 4.08 km/s; western branch, 3.93 km/s; eastern branch, 3.79 km/s; and background, 3.94 km/s. Transects A-A′ and B-B′ correspond to vertical profiles shown in Figure 11. (b) Results from 2-D inversion for phase velocity using Figure 6a as the starting model. Phase velocity, *C* (km/s), gray scale corresponds to Figures 6a and 6b. (c) Standard deviations for phase velocity map shown in Figure 6b. Contour interval is 0.01 km/s. (d) Phase velocities results in Figure 6b subtracted from the starting model in Figure 6a and normalized by the standard deviation shown in Figure 6c. See color version of this figure at back of this issue.

the 2-D model strongly resembles the starting model, although there are some noticable changes. In the western branch of the rifts, velocities are slower in the vicinity of Lake Malawi and faster near Lake Tanganyika compared to the starting model. At the SE corner of the craton the gradients along the craton boundary decrease resulting in lower velocities than the starting model in the craton interior. These lower gradients are observed for all periods less than 100 s. Velocities are higher than the starting model east of the craton at about 4°S.

[21] The map in Figure 6d shows the difference between the 2-D model (Figure 6b) and the starting model (Figure 6a), normalized by the a posteriori standard model errors (Figure 6c). Anomalies in this ratio indicate the regions where the data forces statistically significant deviations from the starting model. The standard errors should not be interpreted as the standard errors of the absolute velocities at individual points in Figure 6b, but rather the uncertainty in the damped and smoothed changes to the starting model averaged over the Gaussian weighted region. In this map, the characteristic averaging length, L_w, where the weights fall to 1/*e* of the maximum value, is 100 km. Because the solution is damped by assigning a priori standard deviations to the starting values [*Tarantola and Valette*, 1982; FL], the absolute values at any point are affected by the starting model. We think the starting model based on a priori regionalization and pure path inversion represents most of the velocity changes in the region. The full 2-D solution indicates whether this assumption is correct and where other variations are required, although the amplitude of these variations is likely to be underestimated. Most of the craton region shows deviations close to zero and indicates little change to the fast velocity craton is required by the data. Likewise, the low velocities assigned to the eastern and

western branches also require little change. The high-velocity anomaly centered at 4°S at the eastern edge of the map approaches 2 standard deviations and may represent a return to "normal" continental lithosphere. The data require low phase velocities for all periods less than 100 s in the SE corner of the craton beneath recent Cenozoic extension faults. Relatively low velocities in this area are consistent with recent surface wave tomography studies [*Debayle et al.*, 2001], a low gravity Bouguer anomaly [*Simiyu and Keller*, 1997], and receiver function data that show a thin upper mantle transition zone beneath the SE corner of the craton [*Owens et al.*, 2000]. We suggest that this low-velocity anomaly indicates recent disruption of the cratonic lithosphere by the rifting process.

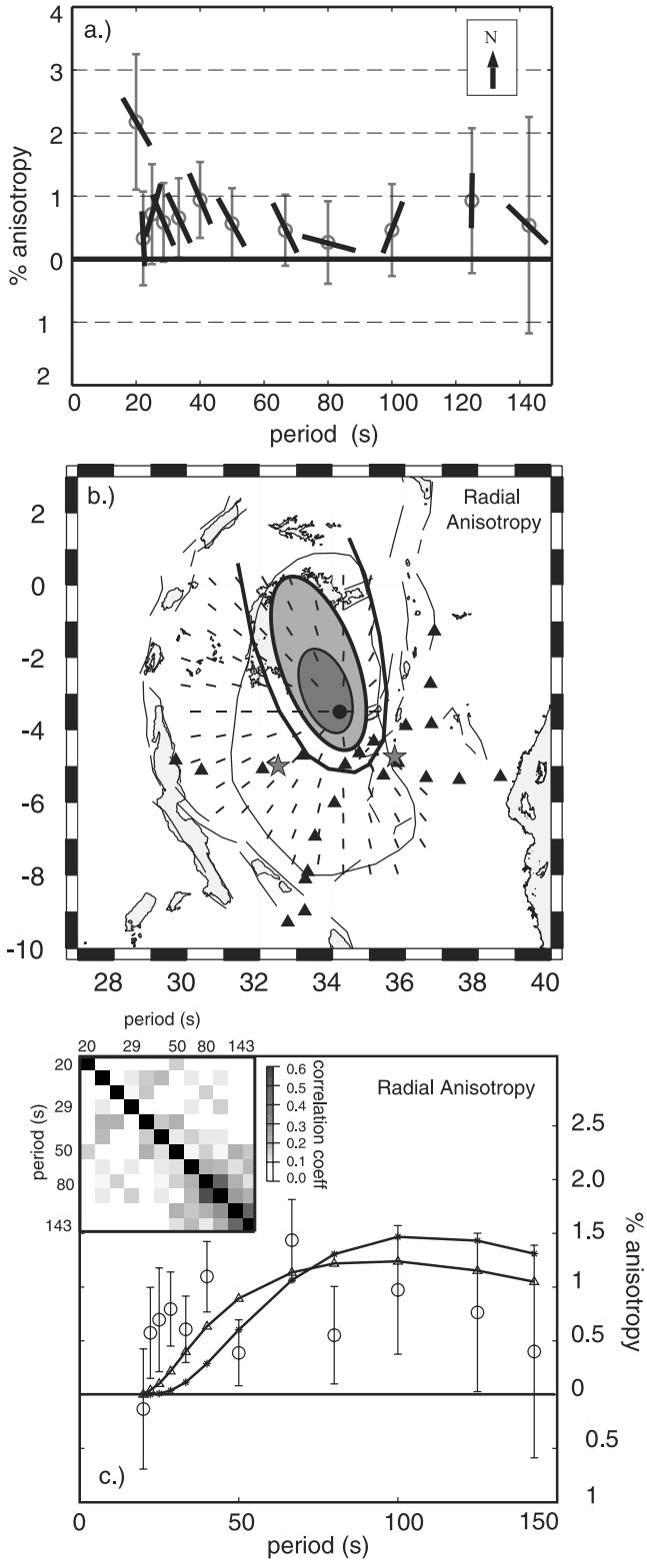

Figure 7. (opposite) (a) Uniform azimuthal anisotropy for the craton region (circles). Thick bars indicate azimuthal orientation in map view. The mean azimuth is 17° west of north ±21°. (b) Anisotropy inversions indicate a center of radial symmetry at a point SE of Lake Victoria surrounded by 68% (dark shading), 95% (light shading), and 99% (solid line parabola) confidence limits. Bars show the predicted fast direction for radially oriented anisotropy. Stations and volcanic centers are shown as in Figure 1. (c) Amplitudes for radial anisotropy compared with forward models of anisotropy prescribed in layer depths 120–300 km (asterisks) and 80–300 km (triangles). Correlation coefficients of residuals between all periods are depicted in the upper left.

[22] Azimuthal anisotropy is considered in several 2-D phase velocity inversions. First, we solve for anisotropy that varies uniformly in two geologic areas: the craton and the remaining study area excluding the craton. We then perform a second set of tests for anisotropy oriented radially about a central point that could represent the vertical axis of an upwelling plume. In the uniform anisotropic inversions, the fast direction is required to be constant within the craton but can vary for each period. Weak anisotropy of less than 1% is observed at most periods (Figure 7a). Although the anisotropy is not different from zero within 95% confidence limits for any one period, the consistency in direction over many periods suggests that it may be real. Except at the longest periods, correlation of residuals in phase (or travel time) between adjacent periods is low (inset in Figure 7c), indicating that each period can be regarded as a nearly independent observation. Thus it is unlikely that a NNW fast direction would be consistent between periods 20 and 80 s (Figure 7a) unless required by the data. This NNW fast direction is consistent with shear wave splitting results at nearby stations NAI and KMBO [*Barruol and Ismail*, 2001] but does not agree with studies in the Kenya Rift, northeast of our study area, where NNE splitting azimuths may be associated with rift parallel mantle flow or magmatic cracks within the rift axes [*Gao et al.*, 1997]. If we assume the best fit azimuth of -17° is correct and fix it at all periods, then we find the weighted average strength of anisotropy over all periods is $0.30 \pm 0.14\%$, taking into account the complete covariance matrix between periods. This average value is very small, but significantly different from zero at the 90% confidence level. Anisotropy for the background region is highly variable and no dominant orientation is resolved.

[23] In order to test previous hypotheses for a mantle plume at the base of the East African Plateau [e.g., *Ebinger et al.*, 1989a; *Simiyu and Keller*, 1997; *Nyblade*, 2002], we consider anisotropy radially distributed about a point. The best plume center location is obtained by a grid search throughout the plateau region between the eastern and western branches. For each inversion, the radial orientation

is fixed about this particular central point for all periods and we find the weighted average amplitude of anisotropy for the plateau region. The best plume center location at approximately 4°S, 34°E (Figure 7b) and the resulting average amplitude, 0.71 ± 0.17%, is a significantly better model than the uniform anisotropy case. In a sense, the uniform anisotropy case is a special case of the radial model with the center of symmetry at infinity. The amplitude of the best uniform model, 0.30 ± 0.14%, lies outside the 95% confidence limits of the best overall model. This same principle of comparing the model amplitude to the amplitude of the best model is used to define the confidence contours for possible location of the center of radial symmetry in fast directions (Figure 7b).

[24] We estimate the depth range over which anisotropy is required, by performing a forward model prescribing uniform anisotropy for a model upper mantle in various depth ranges [*Thomson*, 1997; *Li et al.*, 2003]. We assume that the mantle is 70% olivine and 30% orthopyroxene and that some fraction of the olivine *a* axes are preferentially oriented in the observed fast direction. We then adjust the fraction of aligned crystals to approximately match the observed degree of azimuthal anisotropy. The predicted amplitude of anisotropy (asterisks and triangles) is compared to our observed value (circles) for each period in Figure 7c. Anisotropy restricted to depths between 120 and 300 km (asterisks) is consistent with our results only for periods greater than 40 s. Allowing anisotropy to extend to shallower depths, between 80 and 300 km (triangles), provides a better fit to amplitudes at all periods and indicates that anisotropy is required within at least the lower lithosphere. An even better fit would be obtained with anisotropy from the base of the crust to 300 km, although depth resolution is poor because the uncertainties are large relative to the observed amplitude of the anisotropy at each period. Although the radial pattern of anisotropy is statistically significant, this pattern of alignment of fast directions is based intuitively on a model of radial flow away from a hot spot that would predict anisotropy only within the asthenosphere. Thus this pattern warrants confirmation from shear wave splitting or other independent evidence.

[25] Checkerboard tests and maps of the resolution matrix for phase velocity parameters give insight into the resolution of lateral variations in the velocity maps. The inversion is successful in recovering lateral velocity variations with wavelengths greater than 200 km but smaller anomalies are not well resolved due to variable ray path coverage. Azimuthal anisotropy may always trade off with small-scale lateral heterogeneities, but we find that there is very little trade-off between average azimuthal anisotropy terms in the inversion and phase velocities at scales greater than 300 km.

4. Regional Shear Wave Velocity Structure

[26] We perform inversions for shear wave velocity using phase velocity results from the four geologic areas. Rayleigh waves depend most strongly on *S* velocity and less strongly on density and *P* velocity. The greatest sensitivity to *P* velocity is within the crust. In our inversions for shear velocity, we fix the ratio of *P*-to-*S* velocity at the value of the starting model, and then combine *P* and *S* sensitivity kernels. The shear wave inversion provides a model of shear wave velocity perturbations to the starting model ak135 [*Kennett et al.*, 1995], which gives the best fit between observed and predicted phase velocities [*Saito*, 1988]. Our models are lightly damped by introducing nonzero terms in the diagonals of the a priori model covariance matrix and lightly smoothed by forcing correlation between model changes of adjacent layers through the introduction of nonzero terms to the off-diagonals [FL].

[27] Our primary interest is in mantle structure, but we also modify the starting model in a grid search to find the crustal velocity and thickness for each geological area that gives the best fit to phase velocity data in a least squares sense. No change in the crustal structure of the original model is required for the craton and background regions, which have a crustal thickness of 34 km and shear wave velocities of 3.46 km/s and 3.85 km/s in the upper and lower crust, respectively. Similar crustal thickness values for the Tanzanian craton were obtained in previous studies [*Rykounov et al.*, 1972; *Tesha et al.*, 1997] and slightly thicker estimates were reported in recent surface wave and receiver function studies [*Last et al.*, 1997]. We find a best fit crustal thickness for the western rift branch of 45 km, consistent with *P* wave arrivals reflected off the base of the crust [*Camelbeck and Iranga*, 1996] and receiver function studies for the station GOMA [*Last et al.*, 1997]. Shear wave velocity is 3.50 km/s for the upper crust and 3.70 km/s for the lower crust. The eastern branch requires a crustal thickness of 40 km, and upper and lower crustal velocities are 3.35 and 3.65 km/s, respectively. Crustal thickness estimates for the eastern branch are consistent with refraction studies [*Birt et al.*, 1997; *Prodehl et al.*, 1997] but are slightly higher than estimates from receiver function studies of the Tanzanian Broadband Experiment (36–39 km) [*Last et al.*, 1997] and may reflect our consideration of a larger area for the eastern branch region (Figure 4). Crustal thicknesses are greater in the rifts than in the craton because the rifts are located in mobile belts in which the crust had been tectonically or magmatically thickened prior to rifting. Recent seismic reflection studies suggested thick layering in the lower crust beneath the Kenya rift thought to be associated with magmatic intrusions and underplating [*Thybo et al.*, 2000] which may lower the shear velocity of the deeper crust. Some uncertainty in crustal thickness is expected because there is a trade-off between thickness and velocities in the lower crust and the uppermost mantle. Results for all regions are consistent with global crustal models that include the East African Rift system [*Mooney et al.*, 1998].

[28] Vertical shear wave velocity profiles are shown in Figure 8 for the four geologic regions. Beneath the craton, velocities from the Moho to about 150 km depth are higher than the ak135 reference model. Beginning at a depth of about 140 km, there is a strong negative velocity gradient leading to velocities as much as 9% lower than ak135 at 250 km depth where $\beta = 4.20 \pm 0.05$ km/s. This low-velocity zone may extend from 140 km to as deep as 350 km. Below 250 km, low *S* velocities compared to ak135 persist beneath the craton independent of our choice for the starting model and suggest that anomalously low *S* velocities may continue into the deeper mantle transition zone, where we lose resolution.

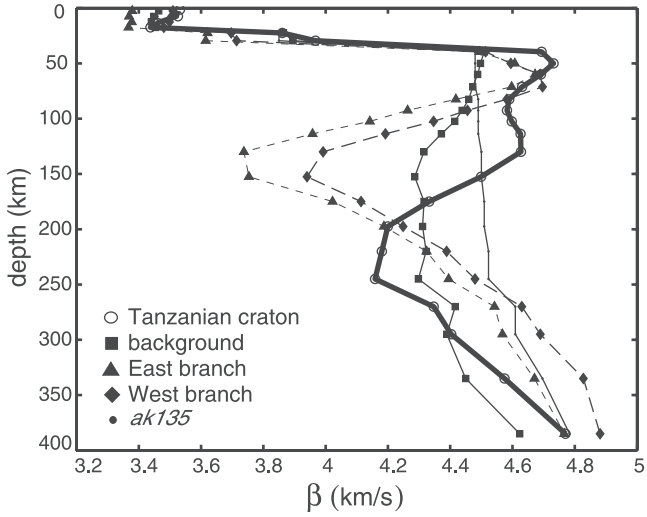

Figure 8. Shear wave velocity profiles for geologic areas using starting model, ak135, (small dots). Profiles are plotted for the craton (circles and bold line), western branch (diamonds and long dashed line), eastern branch (triangles and short dashed line), and background (squares). Symbols correspond to those in Figure 4.

[29] Rank and resolution lengths for the geologic area inversions are a measure of what we are able to resolve about vertical distribution of shear wave velocity in our models. Rank is a description of the number of independent pieces of information about the model provided by the data. Inversions for the craton have the highest rank of 4.9, and inversions for the rifts show rank of 3.0. The rank for the craton is higher than for other regions because the uncertainty in the phase velocities is much smaller (Figure 5a). Resolution length is a measure of the depth range in the model over which the average velocity is well resolved, i.e., the number of layers that need to be combined for the rank of that part of the resolution matrix to be equal to 1.0. For example, at 40 km depth, a 20 km thick layer is required to recover one independent piece of information about velocity. At 70 km depth, resolution length increases to 33 km, and at 150 and 300 km the length is 62 and 170 km, respectively. Resolution kernels are plotted in Figure 9 and show how model parameters at a particular depth depend on information from adjacent depth layers. The increasing resolution length with depth is due to the form of the phase velocity kernels shown in Figure 3a. Phase velocities at 125 s, for example, have a peak sensitivity at ~200 km but are influenced by shear velocity over a broad depth range, while shorter periods are sensitive to a much more limited depth range in the uppermost mantle, yielding better control on the upper parts of our models. In the craton, vertical resolution at depths less than 200 km is significantly better in this study then in most other surface wave studies because we extend the analysis to shorter periods, the large number of paths in a small area yields smaller uncertainties in the phase velocity, and the allowance for heterogeneity in the incoming wave field gives a better fit to the observed phases, reducing the variance. At depths greater than 200 km, vertical variations in velocity can be affected by the limitations in horizontal resolution; the long wavelengths of surface waves that sample these depths means that the Fresnel zones are wide and there should be some lateral smearing in response to structure beyond the craton boundaries. Our inversion for phase velocities, however, takes into account the broadening of the region of sensitivity with increasing period, so there should be little bias in the characteristic craton velocities, yielding constraints on cratonic structure to depths of at least 350 km. Other surface wave studies of larger regions that include the Tanzanian craton have employed higher modes or even longer periods with larger wavelengths that are sensitive to greater depths, but those studies also used horizontal smoothing that limits the resolution of deep structure directly beneath the craton.

[30] Interpretation of the velocity model in terms of lithosphere/asthenosphere requires defining a criterion for determining lithospheric thickness. Some authors have used the depth to which a 1% or 0.5% fast velocity anomaly persists. With this definition, vertical smearing of a velocity anomaly can lead to an overestimate of thickness, particularly if the velocity anomaly in the upper lithosphere is underestimated due to damping, and the depth extent is dependent on the value chosen for the velocity threshold. This approach is commonly adopted in body wave tomography because such studies yield good measures of lateral variations in velocity, but poor resolution of the absolute velocity or true vertical velocity gradient. If the lithosphere/asthenosphere transition in the Tanzanian craton were a gradual thermal transition, then the top of the negative velocity gradient at 140 km (Figure 8) might best be identified as the base of the lithosphere. However, if there were a velocity discontinuity at the base of the lithosphere due to onset of melting or increase in water content or change in composition, then the inherent vertical averaging would mean that the beginning of the negative velocity gradient would underestimate the thickness. We adopt the depth to the maximum negative velocity gradient, or in our case the depth to the center of this maximum, as the best estimate of the depth to the base of the lithosphere; a criterion frequently employed in surface wave studies of

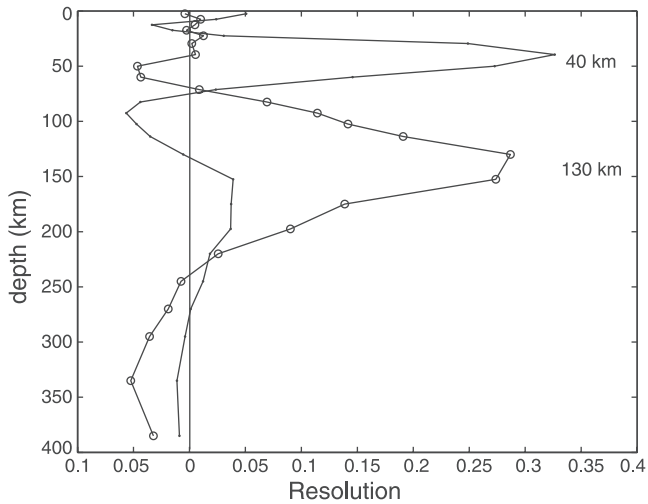

Figure 9. Resolution kernels for shear wave inversions of the craton region shown at 40 km (small dots) and 130 km depth (circles).

both oceanic and continental settings. With this criterion, our estimate of lithospheric thickness is about 170 km. Because the low-velocity zone is so pronounced beneath the Tanzanian craton, all of the criteria described above lead to similar estimates, with lithospheric thickness being uncertain to no more than 20 to 30 km.

[31] Lithospheric velocities beneath the western and eastern branches are similar to the craton, in agreement with the only modest reductions in *Pn* velocities in the rifts [*Brazier et al.*, 2000; *Langston et al.*, 2002]. The onset of the negative velocity gradient begins around 70 km depth in the eastern branch and at about 80 km in the western branch. The lowest velocities in the region are observed beneath the lithosphere of the eastern branch decreasing rapidly from 4.7 km/s at 70 km to 3.7 km/s at 150 km. The low-velocity anomalies below the western and eastern branches are 12–20% lower than beneath the craton at depths of 120–160 km. The low-velocity zone extends at least to depths of 275 km but resolution in the rifts is compromised due to decreased ray path coverage which results in strong dependence on the starting model below 250 km. Body wave tomography [*Ritsema et al.*, 1998] also reported that the lowest velocities were in the rifts at depths of 100–150 km. However, the maximum velocity contrast between the rift branches and the craton was cited as 5–6%. Our results suggest body wave tomography studies may underestimate the magnitude of lateral velocity contrast due to effects of model damping and vertical smearing. In our models, the velocity contrast between craton and rifts reverses at depths of 200–250 km. Assuming vertical smearing in body wave models causes averaging over depths of 100–250 km, the comparable velocity contrast in our models averaged over this same range, is 7–8%.

[32] The background region shows no influence of a high-velocity lithosphere and is close to the starting model above 90 km depth. Low velocities compared to the starting model are observed at depths between 100 and 250 km and indicate that lower than average velocities may be broadly distributed throughout the study area. Damping of model parameters forces shear wave velocity profiles to follow the starting model when there is little information provided by the data. Since there is more information for the craton profile due to smaller errors in phase velocity, the observations can force changes in the cratonic model at greater depths. We test whether the apparent fast velocities from 250 to 400 km depth beneath the rifts are required by using the craton velocity structure as a starting model within the rifts. We find that the differences between rift and craton in this depth range are not significant. The shear velocity profile in the craton region, however, is little influenced by changes in the starting model due to well-constrained phase velocity data at all periods (Figure 5a). Therefore low velocities are required beneath the craton below 250 km and are possible but not required beneath the rifts due to larger uncertainty in phase velocity in the rifts.

[33] In order to compare velocity structure in the Tanzanian craton with other Archean lithosphere, we perform shear wave velocity inversions of data obtained from global maps of fundamental mode Rayleigh wave phase velocities (Figure 5d) at frequencies between 6.6 and 28.5 mHz [*Ekstrom et al.*, 1997] for continental regions composed of Archean crustal rocks. The starting model for all global profiles is the same model used for the Tanzanian craton region in Figure 8. High-velocity lithosphere compared to the global average ak135 model like that of the Tanzanian craton is observed for the Kaapvaal, Canadian, western Siberian, Yilgarn, and Amazonian cratons and extends to depths (defined by the maximum negative gradient) ranging from 160 to 180 km (Figure 10). Below 250 km, *S* velocities closely follow the global mantle average down to 400 km. A subtle low-velocity zone is observed for all craton models, at depths ranging from 150 to 250 km, indicating the transition between the base of high-velocity cratonic lithosphere and deeper global average mantle where deviations from ak135 reach ~4%. Lithospheric thickness obtained from this global data set is consistent with studies of the Canadian shield using *SH* waves [*Grand and Helmberger*, 1984] and surface wave studies of the Kaapvaal craton [*Freybourger et al.*, 2001; *Saltzer*, 2002], but it is thinner than estimates from body wave tomography that typically identify the base of the lithosphere by the maximum depth to a threshold velocity difference [*Frederiksen et al.*, 2001; *James et al.*, 2001; *van der Lee*, 2002]. The velocity of the Indian shield lithosphere is not as high as other Archean cratons. Both the Indian and the eastern Siberian shields appear to have stronger low-velocity zones below 150 km than is observed beneath most cratonic lithosphere but do not reach *S* velocities below 4.40 km/s. The Sino-Korean craton has *S* velocities lower than ak135 at depths up to 250 km below which it follows the starting model, indicating the absence of a typically thick subcratonic lithosphere. The tendency of global profiles to follow the starting model at deeper depths may represent decreased resolution of fundamental mode Rayleigh waves in the surface wave data set below 250 km [*Ekstrom et al.*, 1997; *Dziewonski and Ekstrom*, 1998]. We try to minimize the effect of variable ray path coverage in the global data set by choosing Archean cratons with large areas, consistent with the resolution limits of the global model. If the base of the lithosphere is identified consistently in surface wave tomography models as the depth of maximum gradient, then this preliminary survey of globally distributed cratonic lithosphere suggests that Archean age lithospheric roots may not extend beyond 200 km depth and the lithosphere of the Tanzanian craton is not exceptional.

[34] Vertical cross sections through the shear wave velocity model of the Tanzanian craton are obtained by combining a series of one dimensional inversions of phase velocities from nodes along a line of interest obtained from two-dimensional phase velocity maps. The grid node spacing only provides a crude estimate of continuously varying velocity but is able to capture useful information of upper mantle structure. Two shear wave velocity cross-sectional profiles shown in Figure 11 extend from A to A′ and B to B′ as depicted in Figure 6a. The dominant feature in Figure 11a is the high-velocity lithosphere beneath the Tanzanian craton extending to approximately 170 km depth. Beneath the western branch, anomalously low velocities are observed at depths down to 180 km. The eastern branch shows the largest low-velocity anomaly in the cross section at approximately 150 km depth, and the low velocities continue to at least 220 km depth. The images in Figure 11 are only rough cartoons that are dominated by the regional structure

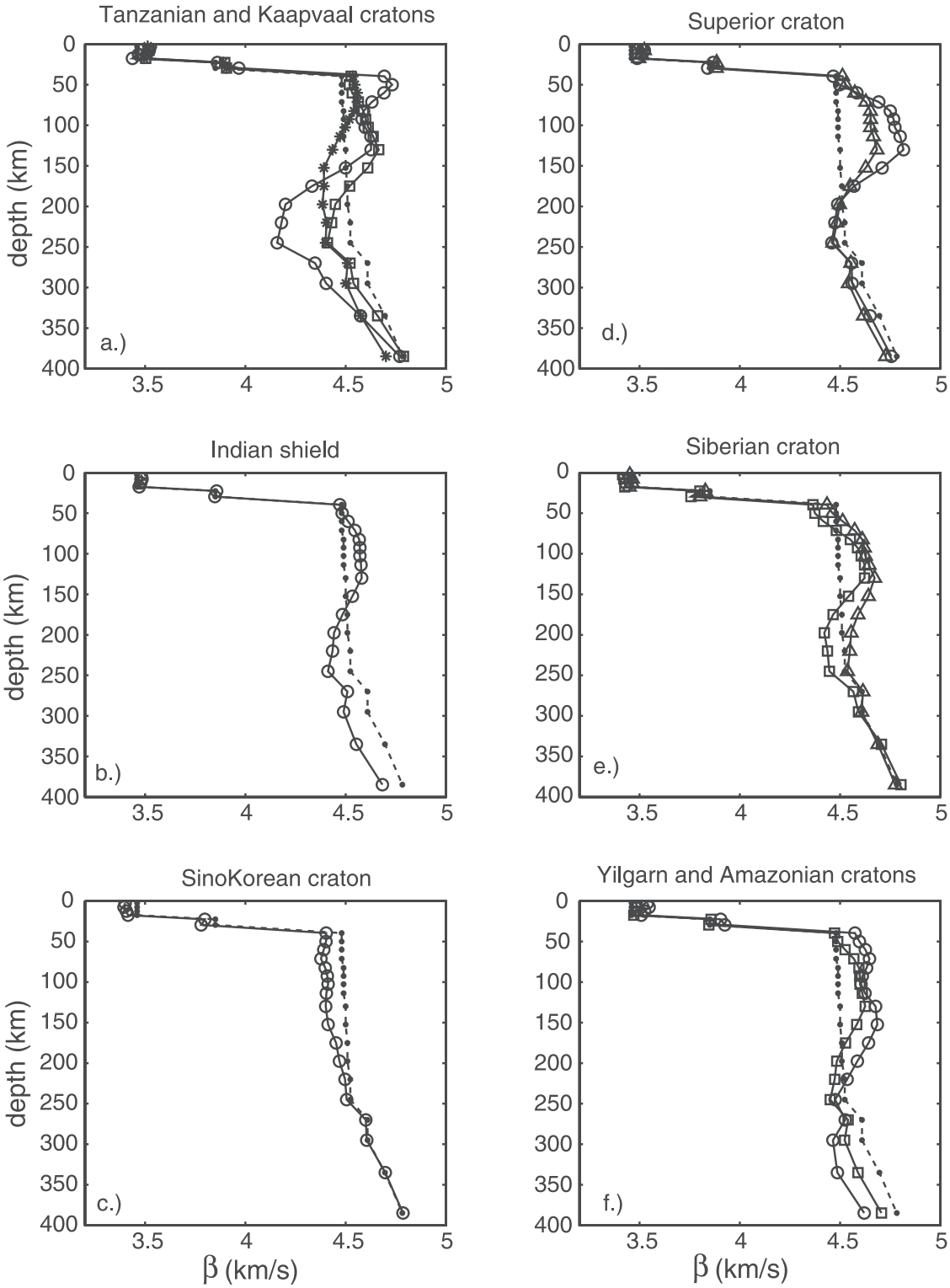

Figure 10. (a) Shear wave velocity profiles for Archean cratons (Figure 5c) based on a global surface wave data set [*Ekstrom et al.*, 1997]. Starting models, ak135 (small dots), have crustal thickness of 34 km and are the same for all profiles. Shear wave velocities obtained for the Tanzanian craton in this study (circles) are compared to inversions of the global data set for Tanzania (asterisks) and the Kaapvaal craton (squares).(b) Indian craton.(c) Sino-Korean craton. (d) Canadian shield shown as southern Superior (triangles) and northern Superior (circles). (e) Siberian craton shown as western Siberia or Anabar (triangles) and eastern Siberia or Aldan (squares). (f) Yilgarn (circles) and Amazonian (squares).

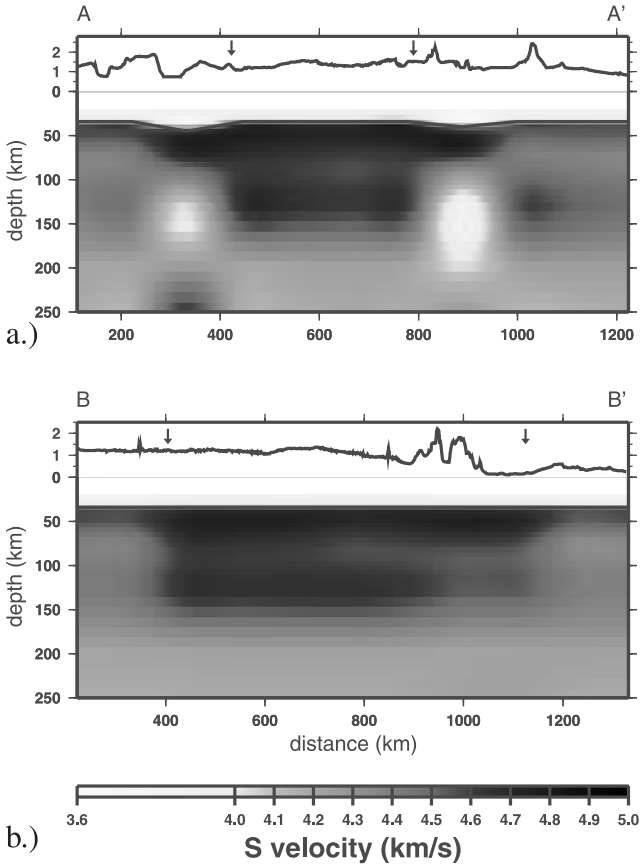

Figure 11. (a) Shear wave velocity cross sections A-A′ as shown in Figure 6a extending from the western rift branch near the Ubendian belt to the Easter rift branch. Moho depth is indicated by solid line below the low-velocity crust. Topography is shown above each cross section. Arrows indicate the Tanzanian craton boundaries. (b) Cross section for B-B′ as shown in Figure 6a extending from the Kibaran belt northwest of the Tanzanian craton to the Usagara belt. See color version of this figure at back of this issue.

models, but they illustrate the overall spatial distribution and magnitude of velocity anomalies seen in the geologic area inversions in Figure 8. One of the interesting deviations from these average area inversions is the reduction in shear velocities in the 100–150 km depth range beneath the southeastern edge of the craton (Figure 11b), which corresponds to the area of reduced phase velocities observed in the two-dimensional phase velocity maps (Figure 6d). The surface location of Cenozoic faulting (Figure 1) which crosscuts the southeastern corner of the Tanzanian craton [*Ebinger et al.*, 1989b] is evident in the topography (Figure 11b) and is coincident with the velocity anomaly, suggesting alteration of the lower lithosphere associated with the minor extension.

5. Stability of Cratonic Lithosphere

[35] The stability of ancient cratonic lithosphere is maintained by the balance of chemical depletion, buoyancy, conductive cooling, and viscous resistance to mantle flow processes [*Jordan*, 1978; *Doin et al.*, 1997; *Jordan*, 1998; *Shapiro et al.*, 1999; *Poudjom Djomani et al.*, 2001]. Petrologic studies confirm the dynamic stability of the Tanzanian cratonic lithosphere. The average density of residual peridotites from the Labait volcano [*Lee and Rudnick*, 1999] is lower than the density of the surrounding asthenospheric mantle and thus counteracts the negative buoyancy of a thermally cold lithosphere, consistent with the isopycnic hypothesis [*Jordan*, 1978]. While many more questions regarding the nature of cratonic stability for the Tanzanian craton have yet to be answered, simply identifying the physical dimensions of the cratonic lithosphere, geochemical composition, and lithospheric age may provide insight into the evolution and longevity of a lithospheric root.

[36] The thickness of the Tanzanian craton appears to be similar to that found in other globally distributed Archean continental lithospheres. Many studies of continental lithosphere demonstrate that there is a negative gradient in velocities below a high-velocity lid at roughly the same depth [e.g., *Grand and Helmberger*, 1984; *Ritsema et al.*, 1998; *Simons et al.*, 1999; *Frederiksen et al.*, 2001; *Saltzer*, 2002; *van der Lee*, 2002]. If we define the base of the lithosphere by the depth of the maximum negative gradient in all studies, we find that Archean lithosphere in general does not appear to exceed 200 km depth and the Tanzanian craton in particular is within the normal population of Archean lithospheres with a mean thickness of about 170 ± 20 km. Our results are consistent with petrologic studies of peridotite xenoliths from adjacent and interior craton volcanoes of the Tanzanian craton where a transition to more fertile asthenospheric mantle begins at depths of 120–140 km [*Griffin et al.*, 1993; *Lee and Rudnick*, 1999; *Chesley et al.*, 1999]. The thickness of the Sino-Korean craton indicated by Figure 10 and in previous xenolith studies [*Menzies et al.*, 1993], however, is anomalous and dramatically departs from the norm, possibly due to past exposure to mantle plume activity [e.g., *Xu*, 2001].

[37] Surface heat flow measurements for the Tanzanian craton are low [*Nyblade et al.*, 1990] but do not directly imply anomalous lithospheric thickness or the absence of thermal anomalies at depth. Heat flow studies of East Africa are hampered by difficulty in isolating crustal and mantle rates of heat production [*Nyblade et al.*, 1990; *Rudnick et al.*, 1998; *Jaupart and Mareschal*, 1998]. Steady state conditions for heat flow may also not have been established. For example, a temperature perturbation at the base of a 100–150 km thick lithosphere is not expected to reach steady state before ~300 Myr [*Nyblade*, 1999]. If the onset time for a perturbation at the base of the Tanzanian lithosphere is associated with rifting, the oldest age for volcanism in the rifts of less than 50 Myr suggests that heat flow conditions are still transient. The heat flow anomaly which is expected even for steady state conditions, however, is within the standard deviation of heat flow measurements [*Nyblade et al.*, 1990; *Nyblade*, 1999] compiled for the East African Plateau and is not an obvious indicator of lithospheric thickness or the presence of thermal anomalies at depth.

[38] The lithosphere of the Tanzanian craton appears to have remained stable throughout its evolutionary history. If a thermal perturbation or plume is present at the base of the craton, the lithosphere has been largely resistant to alteration

except at the southeastern corner where it has been disrupted by rifting. Thermal evolution of the Tanzanian craton may be compared to the more evolved lithospheric erosion of the Sino-Korean craton. Present-day heat flow measurements in the Sino-Korean craton are more than double those obtained for the Tanzanian craton and petrologic studies of xenoliths suggest the Sino-Korean cratonic lithosphere that extended to 180 km depth in the Paleozoic, approximately 400 Ma [*Xu*, 2001], is now virtually absent. One mechanism for stability of the Tanzanian lithosphere is suggested by the presence of mobile and thrust fold belts peripheral to the Tanzanian craton as well as many other Archean continental cratons (e.g., the Amazonian, Indian, and Superior cratons). Numerical models of mantle convection with continental plates suggest that mobile belts may act to ''protect'' cratonic lithosphere by taking up strain from tectonic activity along zones of weakness [*Lenardic et al.*, 2000].

[39] The only evidence of alteration of the cratonic lithosphere that we observe is near the southeastern corner of the craton where shear wave velocities of the lower lithosphere are significantly reduced, although high lithospheric velocities persist to at least a depth of 60 km (Figure 11b). Body wave studies also show modification and lithospheric thinning of the eastern edge of the craton near the Labait volcano [*Nyblade et al.*, 2000]. Lithospheric erosion or alteration thus appears to occur by upward penetration of melt or asthenosphere associated with rifting, rather than by widespread vertical thinning at the base of the lithosphere. While a recent study suggests that the cohesion of the cratonic lithosphere has forced the extensional stresses in the eastern branch to jump to the west side of the craton [*Nyblade and Brazier*, 2002], the Tanzanian craton nonetheless demonstrates limitations in lithospheric stability in the presence of continental rifting.

6. Low-Velocity Anomalies Beneath Archean Lithosphere

[40] The observation of low-velocity zones beneath cratonic lithosphere is not uncommon. Seismic tomography studies for the Kaapvaal craton [*Green et al.*, 1992; *Cichowicz and Green*, 1992; *Freybourger et al.*, 2001; *Saltzer*, 2002], the Canadian Shield [*Grand and Helmberger*, 1984], and the Australian shield [*Simons et al.*, 1999] indicate negative gradients in the velocity profile associated with the transition from high-velocity cratonic lithosphere to global average mantle at greater depths. The low-velocity anomalies below these lithospheric roots, however, do not reach shear wave velocities below 4.4 km/s. By comparison, the dramatic excursion to $\beta = 4.20 \pm 0.05$ km/s at 200–250 km below the surface of the Tanzanian craton is unique. These velocities are lower than velocities found at comparable depths beneath the East Pacific Rise spreading center [*Nishimura and Forsyth*, 1989] and require unusually high temperatures and perhaps partial melting that may be associated with the spreading of a mantle plume head.

[41] A study of the velocity structure beneath Tanzania using stacked receiver functions and *P-S* conversions found an anomalously thin mantle transition zone extending in a band across much of the craton at about 5°S (Figure 2) [*Owens et al.*, 2000], suggesting high temperatures at depths exceeding 410 km. This thermal anomaly may be linked with the low velocities observed beneath the Kenya Rift [*Nyblade et al.*, 2000]. While the thin transition zone indicates a thermal perturbation, this assignment of the thinning due solely to deflection of the 410-km discontinuity was based on body wave tomography results that we believe underestimate the *S* velocity anomaly beneath the craton [*Ritsema et al.*, 1998; *Owens et al.*, 2000]. The travel time from the 410-km discontinuity to the 660-km discontinuity is constrained by *P*-to-*S* converted waves, but if the overlying velocity anomaly is reduced, the transition zone could be shallower because the travel time to the surface is known. We find lower velocities in the overlying mantle could lead to an upward shift of the transition zone relative to the model of *Nyblade et al.* [2000], creating topography on the 660-km discontinuity. A thermal perturbation, therefore, may be present at 660 km or deeper. However, the average transition zone thickness across Tanzania reported by *Nyblade* [2002] is 253 km, consistent with the global average transition zone thickness. Consequently, if a thermal perturbation extends deeper than 660 km, then it probably does not do so uniformly across Tanzania. The decreased width of the thermal anomaly at this depth thus may resemble a narrow conduit or plume tail.

[42] Low-velocity anomalies beneath East Africa have also been observed in the lower mantle by global tomography studies possibly extending from the 660-km discontinuity to depths near the core-mantle boundary [e.g., *Grand et al.*, 1997; *Ritsema et al.*, 1999]. A lower mantle anomaly lends support to the African superswell hypothesis which attributes the elevated topography of east and southern Africa and anomalously shallow bathymetry of the South Atlantic seafloor to a broad mantle plume source in the lower mantle [e.g., *Nyblade and Robinson*, 1994; *McNutt*, 1998; *Lithgow-Bertelloni and Silver*, 1998].

[43] *Ebinger and Sleep* [1998] hypothesized that a single large plume rising beneath the Ethiopian Plateau can explain the distribution and timing of magmatism and uplift throughout east Africa. In this model, the plume spreads laterally beneath the lithosphere, ponding and flowing beneath preexisting zones of lithospheric thinning. A thick Tanzanian lithosphere, therefore, would direct plume material around its perimeter [*Sleep et al.*, 2002]. While channelling of flow can account for low velocities beneath the rifts, it does not predict the low velocities that we observe beneath the craton. Our results may be consistent, however, with this channelled flow hypothesis if the hot spot source is beneath the Tanzanian craton today. Plate motion calculations show that the African plate moved northeastward over the Ethiopian hot spot, bringing the hot spot location over the last 45 Myr from the Main Ethiopian Plateau to near the northern edge of the Tanzanian craton at ~5°N, 37°E [*Sleep et al.*, 2002]. If the plume was not fixed or the plate motion model were in error by a few degrees, their hypothesized, single, large plume could lie beneath the craton near the center for radial anisotropy predicted in this study (Figure 7b). Our strongest evidence for an upwelling mantle plume, however, is the extraordinarily low velocities beneath the cratonic lithosphere, rather than the possible center of symmetry for anisotropy. Whether or not it is the same as the plume invoked by *Ebinger and Sleep* [1998], these anomalous velocities extending to depths of 350 km

or more are best explained by the spreading of a plume directly beneath the craton.

7. Summary

[44] We present evidence for anomalously low velocities beneath the Tanzanian cratonic lithosphere. As crustal thickness estimates obtained here and in previous studies [e.g., *Last et al.*, 1997] are not extraordinary and do not explain the anomalous elevation of the plateau, these low velocities are the first seismic evidence for anomalous structure in the upper mantle that is consistent with the plateau uplift and the pattern of long-wavelength, low Bouguer gravity anomalies on the East African Plateau [*Ebinger et al.*, 1989a; *Simiyu and Keller*, 1997]. The depth to the base of the cratonic lithosphere of about 170 km is consistent with a transition to younger, more fertile asthenosphere suggested for mantle xenoliths from the Labait volcano [*Lee and Rudnick*, 1999; *Chesley et al.*, 1999]. In conjunction with receiver function studies from the Tanzanian Broadband Experiment [*Owens et al.*, 2000] which indicate a thin transition zone, the anomalously low velocities and possible radial pattern of anisotropy support the hypothesis that a plume rises beneath the Tanzanian craton, undergoes partial melting, and spreads out beneath the adjacent eastern and western branches of the East African Rift. While rifting at the craton perimeter has eroded the edge of the original craton boundary, the Archean lithosphere as a whole demonstrates remarkable stability in the presence of upwelling plume activity.

[45] **Acknowledgments.** This work was supported by NSF grant EAR-9903026. Data from the Tanzanian Broadband Experiment were provided by the IRIS data management center. GMT software was used to generate many of our figures. We thank Jeroen Ritsema and two anonymous reviewers for helpful comments that improved this manuscript. Aibing Li and Cindy Ebinger also provided useful discussion.

References

Barruol, G., and W. B. Ismail, Upper mantle anisotropy beneath the African IRIS and Geoscope stations, *Geophys. J. Int.*, *146*, 549–561, 2001.

Birt, C. S., P. K. H. Maguire, M. A. Khan, H. Thybo, G. R. Keller, and J. Patel, The influence of pre-existing structures on the evolution of the southern Kenya rift valley—Evidence from seismic and gravity studies, *Tectonophysics*, *278*, 211–242, 1997.

Brazier, R. A., A. A. Nyblade, and C. A. Langston, *Pn* wave velocities beneath the Tanzanian craton and adjacent rifted mobile belts, East Africa, *Geophys. Res. Lett.*, *27*, 2365–2368, 2000.

Brune, J., and J. Dorman, Seismic waves and earth structure in the Canadian Shield, *Bull. Seismol. Soc. Am.*, *53*, 167–209, 1963.

Cahen, L., N. J. Snelling, J. Delhal, and J. R. Vail, *The Geochronology and Evolution of Africa*, Clarendon, Oxford, U. K., 1984.

Camelbeeck, T., and M. D. Iranga, Deep crustal earthquakes and active faults along the Rukwa trough, eastern Africa, *Geophys. J. Int.*, *124*, 612–630, 1996.

Chesley, J. T., R. L. Rudnick, and C. T. Lee, Re-Os systematics of mantle xenoliths from the East African Rift: Age, structure, and history of the Tanzanian craton, *Geochim. Cosmochim. Acta*, *63*, 1203–1217, 1999.

Cichowicz, A., and R. W. E. Green, Tomographic study of upper-mantle structure of the south African continent, using wave-form inversion, *Phys. Earth Planet. Inter.*, *72*, 276–285, 1992.

Condie, K. C., *Archean Crustal Evolution*, Elsevier Sci., New York, 1994.

Dawson, J. B., Quaternary kimberlitic volcanism on the Tanzania Craton, *Contrib. Mineral Petrol.*, *116*, 473–485, 1994.

Debayle, E., J. J. Lévêque, and M. Cara, Seismic evidence for a deeply rooted low-velocity anomaly in the upper mantle beneath the northeastern Afro/Arabian continent, *Earth Planet. Sci. Lett.*, *193*, 423–436, 2001.

Doin, M. P., L. Fleitout, and U. Christensen, Mantle convection and stability of depleted and undepleted continental lithosphere, *J. Geophys. Res.*, *102*, 2771–2787, 1997.

Dziewonski, A. M., and D. L. Anderson, Preliminary reference Earth model, *Phys. Earth Planet. Inter.*, *25*, 297–356, 1981.

Dziewonski, A. M., and G. J. Ekstrom, Seismic tomography and continental roots (abstract), *Eos Trans. AGU*, *79*(17), Spring Meet. Suppl., S227, 1998.

Ebinger, C. J., and N. H. Sleep, Cenozoic magmatism throughout east Africa resulting from impact of a single plume, *Nature*, *395*, 788–791, 1998.

Ebinger, C. J., T. D. Bechtel, D. W. Forsyth, and C. O. Bowin, Effective elastic plate thickness beneath the East African and Afar Plateaus and dynamic compensation of the uplifts, *J. Geophys. Res.*, *94*, 2883–2901, 1989a.

Ebinger, C. J., A. L. Deino, R. E. Drake, and A. L. Tesha, Chronology of volcanism and rift basin propagation: Rungwe volcanic province, east Africa, *J. Geophys. Res.*, *94*, 15,785–15,803, 1989b.

Ebinger, C., Y. Poudjom Djomani, E. Mbede, A. Foster, and J. B. Dawson, Rifting Archaean lithosphere: The Eyasi-Manyara-Natron rifts, East Africa, *J. Geol. Soc.*, *154*, 947–960, 1997.

Ekstrom, G., J. Tromp, and E. W. Larson, Measurements and global models of surface wave propagation, *J. Geophys. Res.*, *102*, 8137–8157, 1997.

Fairhead, J. D., and R. W. Girdler, The seismicity of Africa, *Geophysics. J. R. Astron. Soc.*, *24*, 271–301, 1971.

Forsyth, D. W., S. C. Webb, L. M. Dorman, and Y. Shen, Phase velocities of Rayleigh waves in the MELT Experiment on the East Pacific Rise, *Science*, *280*, 1235–1238, 1998.

Foster, A. N., and J. A. Jackson, Source parameters of large African earthquakes; implications for crustal rheology and regional kinemats, *Geophys. J. Int.*, *134*, 422–448, 1998.

Frederiksen, A. W., M. G. Bostock, and J. F. Cassidy, *S*-wave velocity structure of the Canadian upper mantle, *Phys. Earth Planet. Inter.*, *124*, 175–191, 2001.

Freybourger, M., J. B. Gaherty, and T. H. Jordan, Structure of the Kaapvaal craton from surface waves, *Geophys. Res. Lett.*, *28*, 2489–2492, 2001.

Friedrich, W., E. Wielandt, and S. Stange, Non-plane geometries of seismic surface wavefields and their implications for regional surface-wave tomography, *Geophys. J. Int.*, *119*, 931–948, 1994.

Gao, S., P. M. Davis, H. Liu, P. D. Slack, and A. W. Rigor, *SKS* splitting beneath continental rift zones, *J. Geophys. Res.*, *102*, 22,781–22,797, 1997.

Grand, S. P., Mantle shear structure beneath the Americas and surrounding oceans, *J. Geophys. Res.*, *99*, 11,591–11,621, 1994.

Grand, S. P., and D. V. Helmberger, Upper mantle shear structure of North America, *Geophys. J. R. Astron. Soc.*, *76*, 399–438, 1984.

Grand, S. P., R. D. van der Hilst, and S. Widiyantoro, Global seismic tomography: A snapshot of convection in the Earth, *GSA Today*, *7*, 1–7, 1997.

Green, W. V., U. Achauer, and R. P. Meyer, A three-dimensional seismic image of the crust and upper mantle beneath the Kenya rift, *Nature*, *354*, 199–202, 1992.

Griffin, W., C. Ryan, S. O'Reilly, P. Nixon, and T. Win, Trace elements in garnets from Tanzanian kimberiltes: Relation to diamond content and tectonic setting, in *Proceedings of the Fifth International Kimberlite Conference: Arax, Brazil, 1991*, vol. 2, edited by H. O. A. Meyer and O. H. Leonardos, pp. 145–147, Comp. de Pesquisa de Recursos Miner., Rio de Janeiro, Brasil, 1993.

Gudmundsson, O., On the effect of diffraction on traveltime measurements, *Geophys. J. Int.*, *124*, 304–314, 1996.

Irvine, G. J., and D. G. Pearson, Lithospheric mantle evolution of the Kaapvaal craton: A Re-Os isotope study of peridotite xenoliths from Lesotho kimberlites, *Geophys. Res. Lett.*, *28*, 2505–2508, 2001.

James, D. E., M. J. Fouch, J. C. VanDecar, and S. van der Lee, Tectospheric structure beneath southern Africa, *Geophys. Res. Lett.*, *28*, 2485–2488, 2001.

Jaupart, C., and J. C. Mareschal, The thermal structure and thickness of continental roots, *Lithos*, *48*, 93–114, 1998.

Jordan, T. H., Composition and development of the continental tectosphere, *Nature*, *274*, 544–548, 1978.

Jordan, T. H., Structure and formation of the continental tectosphere, *J. Petrol.*, Special Lithosphere Issue, 11–37, 1998.

Kampunzu, A. B., M. G. Bonhomme, and M. Kanika, Geochronology of volcanic rocks and evolution of the Cenozoic western branch of the East African Rift System, *J. Afr. Earth Sci.*, *26*, 441–461, 1998.

Kennett, B. L. N., E. R. Engdahl, and R. Buland, Constraints on seismic velocities in the Earth from traveltimes, *Geophys. J. Int.*, *122*, 108–124, 1995.

Langston, C. A., A. A. Nyblade, and T. J. Owens, Regional wave propagation in Tanzania, East Africa, *J. Geophys. Res.*, *107*(B1), 2003, doi:10.1029/2001JB000167, 2002.

Last, R. J., A. A. Nyblade, C. A. Langston, and T. J. Owens, Crustal structure of the East African Plateau from receiver functions and

Rayleigh wave phase velocities, *J. Geophys. Res.*, *102*, 24,469–24,483, 1997.

Lee, C. T., and R. L. Rudnick, Compositionally stratified cratonic lithosphere: Petrology and geochemistry of peridotite xenoliths from the Labait volcano, Tanzania, in *Proceedings of VIIth International Kimberlite Conference*, edited by J. J. Gurney et al., pp. 503–521, Red Roof Design, Cape Town, South Africa, 1999.

Lenardic, A., L. Moresi, and H. Muehlhaus, The role of mobile belts for the longevity of deep cratonic lithosphere: The crumple zone model, *Geophys. Res. Lett.*, *27*, 1235–1238, 2000.

Li, A., D. W. Forsyth, and K. M. Fischer, Shear velocity structure and azimuthal anisotropy beneath eastern North America from rayleigh wave inversion, *J. Geophys. Res.*, *108*(B8), 2362, doi:10.1029/2002JB002259, 2003.

Lithgow-Bertelloni, C., and P. G. Silver, Dynamic topography, plate driving forces and the African superswell, *Nature*, *395*, 269–272, 1998.

Marquering, H., G. Nolet, and F. A. Dahlen, Three-dimensional waveform sensitivity kernels, *Geophys. J. Int.*, *132*, 521–534, 1998.

McNutt, M. K., Superswells, *Rev. Geophys*, *36*, 211–244, 1998.

Menzies, M. A., W. Fan, and M. Zhang, Palaeozoic and Cenozoic lithoprobes and the loss of >120 km of Archaean lithosphere, Sino-Korean craton, China, in *Magmatic Processes and Plate Tectonics*, edited by H. M. Prichard et al., *Geol. Soc. Spec. Publ.*, *76*, 71–81, 1993.

Mooney, W. D., G. Laske, and T. G. Masters, CRUST 5.1: A global crustal model at 5° × 5°, *J. Geophys. Res.*, *103*, 727–747, 1998.

Morley, C. K., Tectonic evolution of the East African Rift system and the modifying influence of magmatism: A review, *Acta Vulcanol.*, *11*(1), 1–19, 1999.

Nishimura, C. E., and D. W. Forsyth, The anisotropic structure of the upper mantle in the Pacific, *Geophys. J.*, *96*, 203–229, 1989.

Nusbaum, R. L., R. W. Girdler, J. R. Heirtzler, D. J. Hutt, D. Green, V. E. Millings, B. S. Schmoll, and J. Shapiro, The distribution of earthquakes and volcanoes along the East African Rift system, *Episodes*, *16*, 427–432, 1993.

Nyblade, A. A., Heat flow and the structure of Precambrian lithosphere, *Lithos*, *48*, 81–91, 1999.

Nyblade, A. A., Crust and upper mantle structure in East Africa: Implications for the origin of Cenozoic rifting and volcanism and the formation of magmatic rifted margins, in *Volcanic Rifted Margins*, edited by M. A. Menzies et al., *Spec. Pap. Geol. Soc. Am.*, *362*, 15–26, 2002.

Nyblade, A. A., and R. A. Brazier, Precambrian lithospheric controls on the development of the East African Rift system, *Geology*, *30*, 755–758, 2002.

Nyblade, A. A., and S. W. Robinson, The African superswell, *Geophys. Res. Lett.*, *21*, 765–768, 1994.

Nyblade, A. A., H. N. Pollack, D. L. Jones, F. Podmore, and M. J. Mushayandebvu, Terrestrial heat flow in east and southern Africa, *J. Geophys. Res.*, *95*, 17,371–17,384, 1990.

Nyblade, A. A., C. Birt, C. A. Langston, T. J. Owens, and R. L. Last, Seismic experiment reveals rifting of craton in Tanzania, *Eos Trans. AGU*, *77*, 517, 521, 1996.

Nyblade, A. A., T. J. Owens, H. Gurrola, J. Ritsema, and C. A. Langston, Seismic evidence for a deep upper mantle thermal anomaly beneath east Africa, *Geology*, *28*, 599–602, 2000.

Owens, T. J., A. A. Nyblade, and C. A. Langston, The Tanzania broadband experiment, *IRIS Newsl.*, *XIV*, 11995.

Owens, T. J., A. A. Nyblade, H. Gurrola, and C. A. Langston, Mantle transition zone structure beneath Tanzania, East Africa, *Geophys. Res. Lett.*, *27*(6), 827–830, 2000.

Polet, J., and D. L. Anderson, Depth extent of cratons as inferred from tomographic studies, *Geology*, *23*, 205–208, 1995.

Poudjom Djomani, Y. H., S. Y. O'Reilly, W. L. Griffin, and P. Morgan, The density structure of subcontinental lithosphere through time, *Earth Planet. Sci. Lett.*, *184*, 605–621, 2001.

Prodehl, C., K. Fuchs, and J. Mechie, Seismic-refraction studies of the Afro-Arabian rift system—A brief review, *Tectonophysics*, *278*, 1–13, 1997.

Ritsema, J., and H. van Heijst, New seismic model of the upper mantle beneath Africa, *Geology*, *28*, 63–66, 2000.

Ritsema, J., A. A. Nyblade, T. J. Owens, C. A. Langston, and J. C. VanDecar, Upper mantle seismic velocity structure beneath Tanzania, East Africa: Implications for the stability of cratonic lithosphere, *J. Geophys. Res.*, *103*, 21,201–21,213, 1998.

Ritsema, J., H. van Heijst, and J. H. Woodhouse, Complex shear wave velocity structure imaged beneath Africa and Iceland, *Science*, *286*, 1925–1928, 1999.

Rudnick, R. L., W. F. McDonough, and R. J. O'Connel, Thermal structure, thickness and composition of continental lithosphere, *Chem. Geol.*, *145*, 395–411, 1998.

Rykounov, L. N., V. V. Sedov, L. A. Sarrina, and V. J. Bourmin, Study of microearthquakes in the rift zones of East Africa, *Tectonophysics*, *15*, 123–130, 1972.

Saito, M., DISPER80: A subroutine package for the calculation of seismic normal-mode solutions, in *Seismological Algorithms: Computational Methods and Computer Programs*, edited by D. J. Doornbos, pp. 293–319, Academic, San Diego, Calif., 1988.

Saltzer, R. L., Upper mantle structure of the Kaapvaal craton from surface wave analysis—A second look, *Geophys. Res. Lett.*, *29*(6), 1093, doi:10.1029/2001GL013702, 2002.

Shapiro, S. S., B. H. Hager, and T. H. Jordan, Stability and dynamics of the continental tectosphere, *Lithos*, *48*, 115–133, 1999.

Simons, F. J., A. Zielhuis, and R. D. van der Hilst, The deep structure of the Australian continent from surface wave tomography, *Lithos*, *48*, 17–43, 1999.

Simiyu, S. M., and G. R. Keller, An integrated analysis of lithospheric structure across the East African plateau based on gravity anomalies and recent seismic studies, *Tectonophysics*, *278*, 291–313, 1997.

Sleep, N. H., C. J. Ebinger, J. M. Kendall, Deflection of mantle plume material by cratonic keels, in *The Early Earth: Physical Chemical and Biological Development*, edited by C. M. R. Fowler, C. J. Ebinger, and C. J. Hawkesworth, *Geol. Soc. Spec. Publ.*, *199*, 135–150, 2002.

Smith, M. L., and F. A. Dahlen, The azimuthal dependence of Love and Rayleigh wave propagation in a slightly anisotropic medium, *J. Geophys. Res.*, *78*, 3321–3333, 1973.

Spetzler, J., and R. Snieder, The effect of small-scale heterogeneity on the arrival time of waves, *Geophys. J. Int.*, *145*, 786–796, 2001.

Tarantola, A., and B. Valette, Generalized non-linear problems solved using the least-squares criterion, *Rev. Geophys.*, *20*, 219–232, 1982.

Tesha, A. L., A. A. Nyblade, G. R. Keller, and D. I. Doser, Rift localization in suture-thickened crust: Evidence from Bouguer gravity anomalies in northeastern Tanzanian, East Africa, structure and dynamic processes in the lithosphere of the Afro-Arabian Rift system, *Tectonophysics*, *278*, 315–328, 1997.

Thomson, C. J., Modeling surface waves in anisotropic structures I. Theory, *Phys. Earth Planet. Inter.*, *103*, 195–206, 1997.

Thybo, H., P. K. H. Maguire, C. Birt, and E. Perchuc, Seismic reflectivity and magmatic underplating beneath the Kenya Rift, *Geophys. Res. Lett.*, *27*, 2745–2748, 2000.

van der Lee, S., High-resolution estimates of lithospheric thickness from Missouri to Massachusetts, USA, *Earth Planet. Sci. Lett.*, *203*, 15–23, 2002.

Xu, Y. G., Thermo-tectonic destruction of the Archaean lithospheric keel beneath the Sino-Korean craton in China: evidence, timing and mechanism, *Phys. Chem. Earth*, *26*, 747–757, 2001.

Zhang, Y. S., and T. Tanimoto, High-resolution global upper mantle structure and plate tectonics, *J. Geophys. Res.*, *98*, 9793–9823, 1993.

K. M. Fischer, D. W. Forsyth, and D. S. Weeraratne, Department of Geological Sciences, Brown University, P.O. Box 1846, Providence, RI 02912-9019, USA. (Karen_Fischer@brown.edu; Donald_Forsyth@brown.edu; Dayanthie_Weeraratne@brown.edu)

A. A. Nyblade, Department of Geosciences, Pennsylvania State University, University Park, PA 16802, USA. (andy@essc.psu.edu)

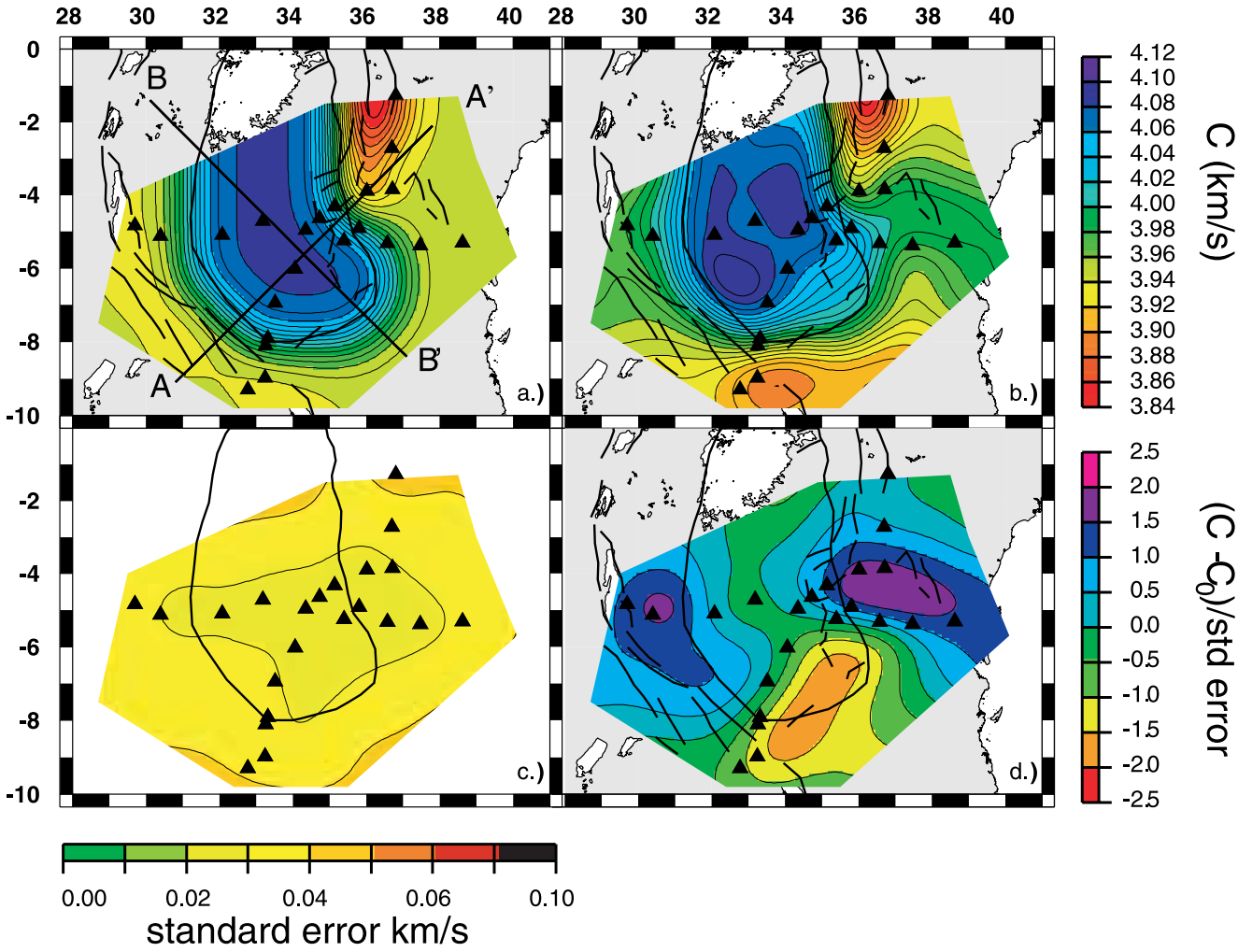

Figure 6. Phase velocity map for 2-D inversion at 50 s. Tanzanian craton outline and rift segments are shown as in Figure 1. Masked region represents area of best ray path coverage. (a) Starting model for 2-D inversions. Starting velocities are uniform for each region: craton, 4.08 km/s; western branch, 3.93 km/s; eastern branch, 3.79 km/s; and background, 3.94 km/s. Transects A-A′ and B-B′ correspond to vertical profiles shown in Figure 11. (b) Results from 2-D inversion for phase velocity using Figure 6a as the starting model. Phase velocity, *C* (km/s), gray scale corresponds to Figures 6a and 6b. (c) Standard deviations for phase velocity map shown in Figure 6b. Contour interval is 0.01 km/s. (d) Phase velocities results in Figure 6b subtracted from the starting model in Figure 6a and normalized by the standard deviation shown in Figure 6c.

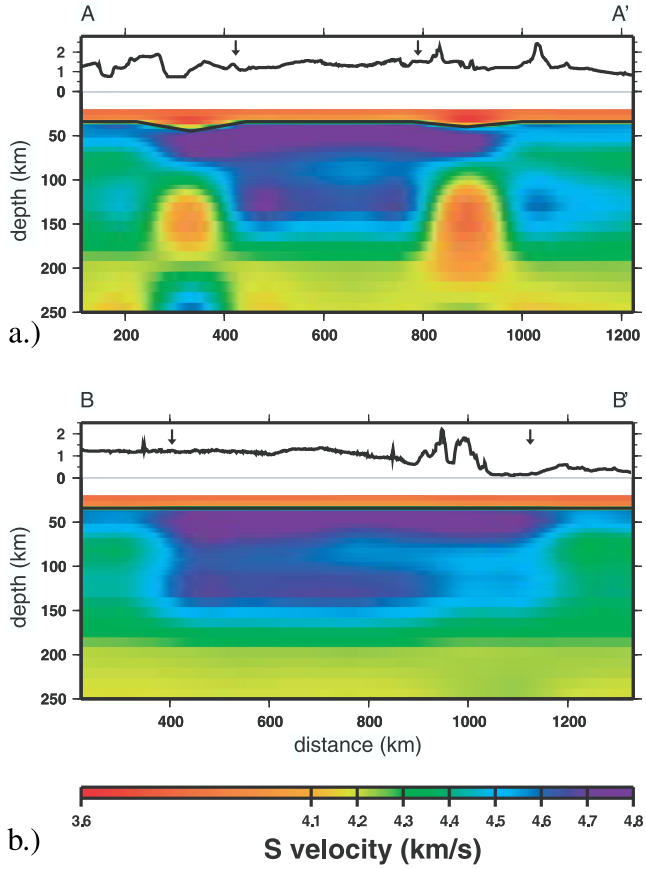

Figure 11. (a) Shear wave velocity cross sections A-A′ as shown in Figure 6a extending from the western rift branch near the Ubendian belt to the Easter rift branch. Moho depth is indicated by solid line below the low-velocity crust. Topography is shown above each cross section. Arrows indicate the Tanzanian craton boundaries. (b) Cross section for B-B′ as shown in Figure 6a extending from the Kibaran belt northwest of the Tanzanian craton to the Usagara belt.